STATE OF CHARGE ESTIMATION OF LITHIUM-ION BATTERY IN MARINE APPLICATIONS

Lappeenranta-Lahti University of Technology LUT

LUT School of Energy Systems

Degree Programme in Electrical Engineering, Master's Thesis

2023

Jyrki Jantunen

Examiners: Full professor (tenured) Pertti Kauranen

M.Sc. (Tech.) Anssi Mattus

ABSTRACT

Lappeenranta-Lahti Univeristy of Technology LUT

LUT School of Energy Systems

Electrical Engineering

Jyrki Jantunen

STATE OF CHARGE ESTIMATION OF LITHIUM-ION BATTERY IN MARINE APPLICATIONS

Master's thesis

2023

66 pages, 30 figures, 9 tables and 3 appendices

Examiners: Full professor (tenured) Pertti Kauranen
M.Sc. (Tech.) Anssi Mattus

Keywords: state of charge (SOC) estimation, lithium-ion battery, marine application, Kalman filter, autoregressive with exogenous input (ARX) model, equivalent circuit

State of charge (SOC) estimation is important for marine battery uses. Running on empty battery on a sea is not an ideal situation, neither is overcharging a battery. SOC is the ratio between the current battery charge and the maximum battery capacity. The challenge of SOC estimation is that it is not directly measurable.

This thesis maps SOC estimation techniques and lithium-ion battery (LiB) models used with them as a literature review. Then a programmable logic controller (PLC) compatible estimation method and model are chosen for implementation. Tests are ran on a LiB to parameterize the selected model and to validate the selected SOC estimation technique so that the absolute error of SOC stays within 20 percentage points.

Steady-state Kalman filter (SSKF) is chosen for implementation because of computational limits. Extended Kalman filter (EKF) is also validated. LiB dynamics are modeled as autoregressive model with exogenous input (ARX). The model is augmented with Coulomb counter and SOC as a function of open circuit voltage (OCV). Both the SSKF and EKF were almost equally accurate, with the EKF being slightly more accurate. The SSKF did not work properly when SOC was under 20 %.

TIIVISTELMÄ

Lappeenrannan–Lahden teknillinen yliopisto LUT

LUT Energiajärjestelmät

Sähkötekniikka

Jyrki Jantunen

Litiumioniakun varaustilan estimointi laivakäytöissä

Diplomityö

2023

66 sivua, 30 kuvaa, 9 taulukkoa ja 3 liitettä

Tarkastajat: Professori (tenured) Pertti Kauranen
Diplomi-insinööri Anssi Mattus

Avainsanat: varaustilan estimointi, litiumioniakku, laivakäyttö, Kalman suodin, autoregressiivinen malli eksogeenisellä tulolla, sijaiskytkentä

Akun varaustilan estimointi on tärkeää laivakäytössä. Akun tyhjeneminen merellä ei ole ideaali tilanne, kuten ei myöskään akun ylilataus. Varaustila on akun tämänhetkisen varauksen ja täyden akun kapasiteetin suhde. Varaustilan estimoinnin haasteena on se, ettei se ole suoraan mitattavissa.

Tässä diplomityössä tutkitaan kirjallisuuskatsauksena erilaisia varaustilan estimointimenetelmiä ja niiden kanssa käytettäviä litiumioniakkujen malleja. Sen jälkeen valitaan implementoitavaksi ohjelmoitavan logiikan kanssa yhteensopiva malli ja estimointimenetelmä. Litiumioniakulla suoritetaan testejä, joilla parametroidaan valittu malli sekä validoidaan estimointimenetelmä. Validoinnilla varmistetaan varaustilan estimaatin absoluuttisen virheen olevan alle 20 prosenttiyksikköä.

Jatkuvuustila Kalman suodin valitaan implementoitavaksi laskennallisten rajoitteiden takia. Sen lisäksi myös laajennettu Kalman suodin validoidaan. Litiumioniakun dynamiikkaa mallinnetaan autoregressiivisella mallilla, jossa on eksogeeninen tulo. Malliin lisätään Coulombi-laskuri ja akun avoimen piirin jännite akun varaustilan funktiona. Molemmat Kalman suotimet ovat lähes yhtä tarkkoja. Laajennettu on hieman tarkempi verrattuna jatkuvuustila Kalman suotimeen, joka ei toiminut enää kunnolla varaustilan ollessa alle 20 %:a.

ACKNOWLEDGMENTS

I want to thank Danfoss for this interesting thesis subject. I'm especially grateful for Anssi Mattus for all the support and advice given during the writing of this thesis. Thanks to all of the Danfoss marine team coworkers for making Danfoss such a great workplace.

I also want to express my gratitude for professor Pertti Kauranen for the great feedback and the given guidance. Thanks to Toni Viinanen for the help with the measurements.

Huge thanks to all my friends. You made my time in Lappeenranta an unforgettable experience and the COVID lockdowns bearable. I'll never forget the online lectures of analogiatekniikka at the friend's cabin. Last but not least, special thanks to the high school friends who helped me with the thesis.

SYMBOLS AND ABBREVIATIONS

Roman characters

A	system matrix	[-]
a	coefficient	[-]
B	input matrix	[-]
b	coefficient	[-]
C	measurement matrix, capacitor, C-rate	[-]
D	feedthrough matrix	[-]
e	error	[-]
i, I	current	[A]
j	imaginary unit	[-]
k	timestep	[-]
R	resistor	[-]
n	nth	[-]
t	time	[s, min, h]
u, U	voltage, input	[V, -]
W	Warburg element	[-]
x	state	[-]
y	output	[-]
Q	charge	[C]

Greek characters

δ, Δ	change	[-]
η	coulombic efficiency	[-]
ω	frequency	[rad/s]
θ	capacity	[F]

Dimensionless quantities

pp	percentage point

Subscripts

d	dynamic
est	estimate
i	index
int	internal
k	timestep
max	maximum
meas	measurement
n	nth
oc	open circuit
ocv	open circuit voltage
p	parallel
s	series, sample
t	terminal

Superscripts

○	degree
+	positive
’	real axis
”	imaginary axis
n	nth

Abbreviations

Ah Ampere-hour

ARX auto-regressive model with exogenous input

BEV battery electric vehicle

BMS battery management system

CC constant current

CDKF central difference Kalman filter

CKF cubature Kalman filter

CPE constant phase element

CV constant voltage

DFN Doyle-Fuller-Newman

ECM equivalent circuit model

EIS electrochemical impedance spectroscopy

EKF extended Kalman filter

EM electrochemical model

EMF electromotive force

EV electric vehicle

HEV hybrid electric vehicle

HPPC hybrid pulse power characterization

KF Kalman filter

LCO lithium cobalt oxide

LFP lithium iron phosphate

LiB lithium-ion battery

LMO lithium manganese oxide

LTO lithium titanate

MAE mean absolute error

MAPE mean absolute percentage error

NMC lithium nickel manganese cobalt

OCV open circuit voltage

PHEV plug-in hybrid electric vehicle

PLC programmable logic controller

PNGV partnership for a new generation of vehicle

RMSE root-mean-square error

SEI solid electrolyte interface

SNR signal-to-noise ratio

SOC state of charge

SSKF steady-state Kalman filter

UKF unscented Kalman filter

TABLE OF CONTENTS

A APPENDIX: ORIGINAL AND PROCESSED DATA

B APPENDIX: POLYNOMIALS

C APPENDIX: RMSE AND MAPE OF DIFFERENT POLYNOMIALS

List of Figures

List of Tables

1 INTRODUCTION

In electric drives, knowing accurate state of charge (SOC) of a lithium-ion battery (LiB) is crucial. For electric vehicle (EV) use, knowing the SOC is like knowing how much fuel is left on a combustion engine car. SOC is defined as the ratio of current capacity to the nominal capacity [1]. Running on empty battery in the middle of nowhere while driving EV is not an ideal situation, neither is overcharging a battery. Or in a marine context, running on a empty battery in the middle of a sea. The challenge of SOC estimation is that it is not directly measurable, thus estimation is required. This thesis explores different kinds of SOC estimation methods.

1.1 Background

LiBs have become the dominant battery technology in the 21st century. Their high specific energy, energy density and specific power make them good for weight and volume restricted applications. LiBs have a low self-discharge rate of 1 % – 5 % per month, depending on the SOC and temperature, long cycle life of 500 – 10 000 cycles and a broad temperature range of operation. These properties allow their use in a wide variety of applications. In addition, LiBs do not have memory effect [2].

There are multiple Li-ion cell chemistries. These chemistries are usually categorized by the cathode material. The first LiBs on the market were lithium cobalt oxide (LCO) batteries. Nowadays there are other less costly materials such as lithium manganese oxide (LMO), lithium nickel manganese cobalt (NMC) and lithium iron phosphate (LFP) [2]. The performance and capacity of different types varies with LCO having the best but also being more expensive. Usually carbon materials are used on the anode but there is an exception. Lithium titanate (LTO) batteries have lithium titanate on the surface of the anode. LTO anode allows for higher charging rates than carbon anode [1], [3].

Often with batteries, discharging and charging currents are represented by C-rate. C-rate represents current relative to a battery's full capacity. For example, a battery with 10 Ah nominal capacity, a current of 1 C means that the current would be 10 A and with 0.1 C would mean that the current is 1 A [1].

When discharging, lithium ions move from the anode (negative electrode) to the cathode (positive electrode) and vice versa when charging, which is shown in Figure 1 [1].

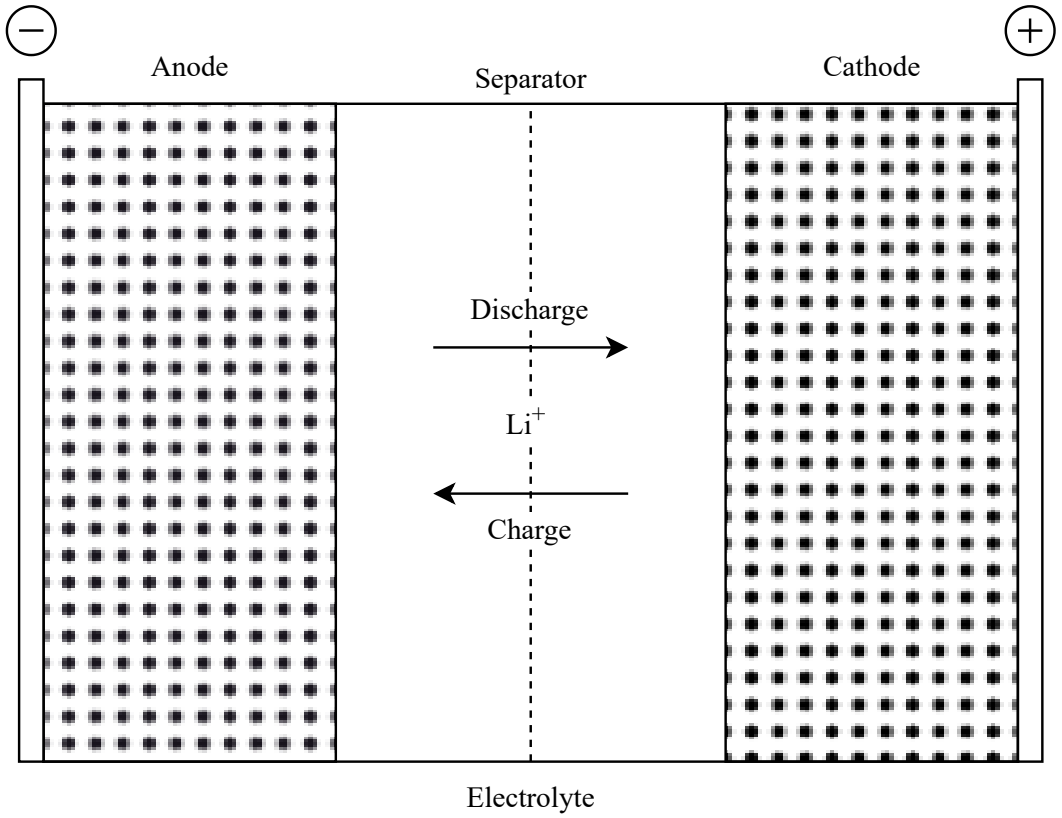

Figure 1: Lithium-ion battery lithium ion movement [1].

When discharging, the lithium ions move from the anode to the cathode through an electrolyte, while electrons move though an external load. When charging, the lithium ions move from the cathode to the anode through the electrolyte.

As LiBs age, their capacity decreases and impedance increases, limiting the power and energy that is available. The production methods of a battery affect its lifetime before actual use. LiBs degrade by cycling (charge and discharge cycles) and by themselves over time and different LiB types age at different rate. External conditions affect a battery's degradation rate. These conditions include temperature, current and charge [4].

Too high and too low temperatures degrade a battery while storing and cycling. A high temperature can lead to battery self heating and thermal runaway. A low temperature increases a battery's impedance [4]. Charging at below 0 °C causes rapid degradation in a LiB. Commercially available cells can be typically charged at 0 °C – 45 °C and discharged at -40 °C – 65 °C [2].

A lower battery SOC benefits a battery's life while a high SOC increases the battery degradation rate. Too low SOC is also bad for a battery. Ideal SOC for battery storage is about 20 %. In a battery electric vehicle (BEV) use, the recommended SOC range is 20 % – 100 %

to maximize the battery life. For hybrid electric vehicle (HEV) and plug-in hybrid electric vehicle (PHEV) it is recommended to cycle the battery in low SOC region, with 30 % – 50 % providing the best battery life [4].

When charging or discharging a battery, the lower the current, the longer the battery life. Higher currents also heat the battery because of Ohmic heating [4]. If a LiB cell is undercharged to below 2 V, it degrades. Overcharging also causes cell degradation and can be dangerous. LiBs do not have a chemical mechanism to protect them from overcharge, thus they need an electrical circuit to protect them from overcharge and overdischarge. It also protects LiBs from being used in too high temperatures [2].

1.2 Objectives, limitations, methods and structure

The main objective of this thesis is to implement a SOC estimation method that has absolute error of less than 20 percentage points (pp) and is implementable on programmable logic controller (PLC). The secondary objective is to gather information about SOC estimation and LiBs for the Danfoss's marine team, which this document serves to fulfill.

The following limitations are set on this thesis:

- PLC realization of SOC estimator is excluded from this thesis.
- Emphasis is placed on more widely used LiB models and SOC estimation techniques.
- Measurement temperatures are not taken into account.

The following research questions need answering to fulfill the objectives:

- Which SOC estimation method is the best suited for PLC offline use?
- Which model is the best fit with the chosen estimation method, if any?

To answer these research questions, a literature review of SOC estimation methods is required. Chapter 2 contains the literature review of SOC estimation methods and LiB models associated with them. Chapter 3 has implementation of the SOC estimator and LiB model along with justifications for chosen the model and estimator. In chapter 4, tests are ran on a LiB to acquire data to parameterize the model and to validate the SOC estimator. The model is parameterized and the estimator results are analyzed in chapter 5. The final conclusions are made in chapter 6.

2 BATTERY MODELING AND STATE OF CHARGE ESTIMATION

SOC estimation methods are divided into two categories, model based and direct estimation methods. The direct methods do not require modeling of a battery but they have drawbacks that may necessitate the use of model based estimation methods. There has been development of new direct estimation methods or improving old ones e.g. Zhang *et al.* have improved the Coulomb counting and Cai *et al.* have used ultrasound to directly measure SOC [5], [6]. The SOC estimation methods can be divided into groups, presented in Figure 2.

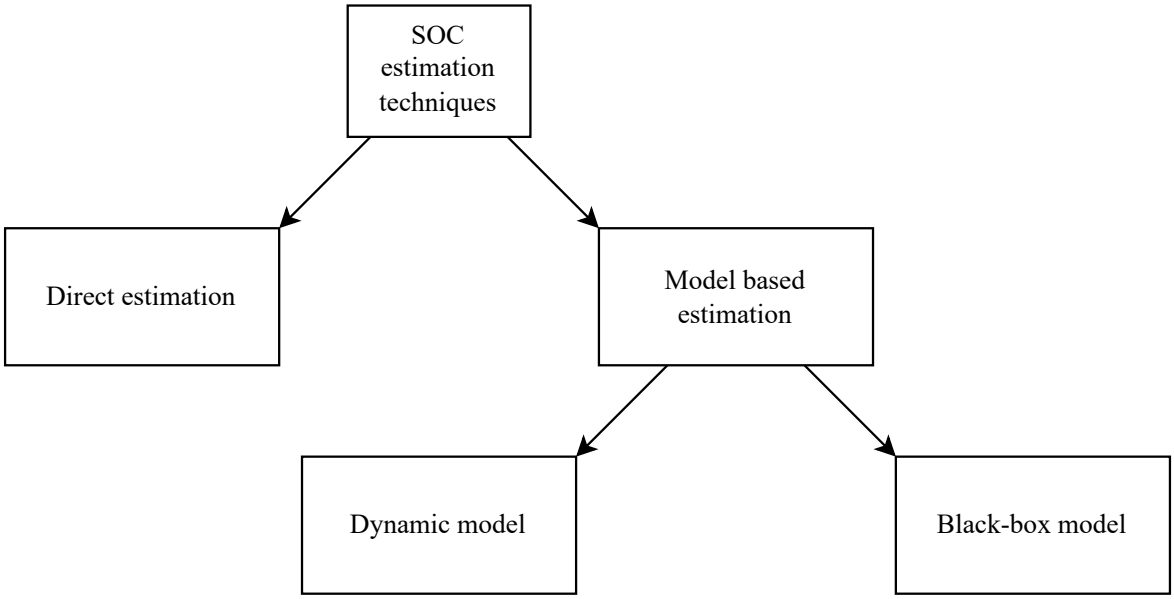

Figure 2: SOC estimation techniques categorized.

The model based estimation methods can be divided into two groups. The first one uses battery models that describe dynamics like electrochemical model (EM) and equivalent circuit model (ECM). In the other group are methods based on black-box models that use machine learning techniques [1], [7]. To get the most efficient SOC estimation, a combination of methods is usually recommended [8].

2.1 Direct estimation

The direct estimation methods are Ampere-hour (Ah) integration and open circuit voltage (OCV)-SOC function. They are called direct estimation methods because they do not rely on a model of a battery [9].

2.1.1 Coulomb counting

The Coulomb counting, also known as Ah integration, was invented in 1975 [10]. As a direct estimation method it is a simple and widely used method to estimate SOC [9]. The Coulomb counting is integrating current over time as is shown in Equation 2.1

$$SOC_k = \frac{\eta}{Q_{max}} \int_{t_0}^{t_k} i(t)\, dt + SOC_0 \tag{2.1}$$

where SOC_k and SOC_0 are the SOC estimates at the time t_k and t_0 with t_0 being the initial moment and $t_k = t_0 + k \times \Delta t$, Δt denotes the sampling interval. η is the Coulombic efficiency for charging, $i(t)$ is the current of the battery with positive for charging and negative for discharging and Q_{max} is the maximum capacity. Usually nominal capacity is used for Q_{max}. However the battery temperature, current and age affect the maximum capacity, causing the actual maximum capacity to differ from the nominal capacity [1], [7].

The Coulomb counting has drawbacks. A noisy measurement and temperature drift in the sensor element cause increasing error in the estimate because of the accumulation of the integral value. Using longer integration time or stronger current reduces the error caused by the noise. The Coulomb counting works the best when a battery is regularly fully charged and discharged at a rate of 1 C or higher, therefore it works better on a BEV than on a HEV or a PHEV. The Coulombic efficiency also increases the error since we cannot use all of the Coulombs that are charged into LiB. LiBs have a efficiency of 0.99 and over thus its effect is small [11]. The initial SOC has to be known when starting Coulomb counting since when integrating, we are estimating the accumulation in charge [7], [9]. We can use the previous SOC value as the initial SOC if battery has been used before. Self-discharge is not an issue since the rate for LiB is about 1 % per month. Because of these drawbacks the Coulomb counting is not usually used by itself but in combination with other estimation methods to re-calibrate the initial and maximum SOC [11]. Improvements to the Coulomb counting have been proposed to increase its accuracy [5], [12]–[14].

2.1.2 OCV-SOC function

Another direct estimation method is the OCV-SOC function. Battery voltage measurement was the first capacity estimation method invented in 1938, with OCV being discovered in 1975. The first OCV-SOC look-up table based method was proposed in 1984 [10]. The SOC of a battery is known to have a monotonic relationship with the electromotive force (EMF) of the battery [15]. By using this knowledge we can determine the SOC by measuring the OCV since it is very close to the EMF of the battery [9]. To form a function of SOC, a discharge

curve provided by battery manufacturer can be used or batteries' OCV-SOC relation can be characterized empirically.

To characterize the OCV-SOC relationship, a battery is charged and discharged fully. Because LiBs have hysteresis, the battery needs to be characterized while charging and discharging to average the measurements and cancel the hysteresis [15]. There are two ways to characterize the OCV-SOC. The first one is charging and discharging a battery at a low current and measuring the voltage [15]. The second one is by using higher currents but before measuring the OCV the battery needs to relax i.e. reach a equilibrium state. The battery's voltage changes until the equilibrium state has been reached, thus the battery is charged and discharged in pulses [9]. The pulse rate and wait time selection depends on the needed accuracy from the model and time available for the measurements [16]. The relaxation time depends on the temperature and the characterization should be done in constant temperature [11]. The relaxation time can take up more than 13 hours for LFP, thus the whole characterization can take days depending on the selected pulse rate and battery chemistry [17].

One of the drawbacks of this method is caused by batteries' internal impedance. The batteries' SOC cannot be estimated when battery is charging or discharging since measuring the OCV while current is going through the battery causes a voltage loss at the terminal. After loading a battery, some time has to be waited for the battery to relax [11]. The second drawback is the hysteresis present in a LiB. Some LiB types e.g. LFP have so flat OCV-SOC curve that even a small measurement error or hysteresis can cause a huge difference in the SOC estimate. Temperature can also cause variance in the OCV-SOC because the capacity is lowered in low temperatures, thus the characterization needs to be done in multiple temperatures that span the battery use range [11]. Research done by Pattipati *et al.* claims that the OCV-SOC can be temperature normalized to remain the same in all temperatures [15].

Usually the Coulomb counting and a OCV-SOC function are used in tandem with each other since the Coulomb counting can be used while there is a current flowing through a battery and the OCV-SOC when the battery is not loaded [9].

2.2 Data-driven estimation and black-box models

Black-box models are models that simulate batteries without knowing their internal electrochemical dynamics. Black-box models utilize data-driven estimation methods to estimate SOC. According to Wang *et al.*, the potential benefits of data-driven methods are adaptability and flexibility to changing conditions and them working well with non-linear systems [18]. Some popular methods that are in use for SOC estimation, such as neural networks, support vector machine, support vector regression, fuzzy logic, Gaussian process regression

and genetic algorithm [19], [20]. The different data-driven estimation methods are presented in Figure 3.

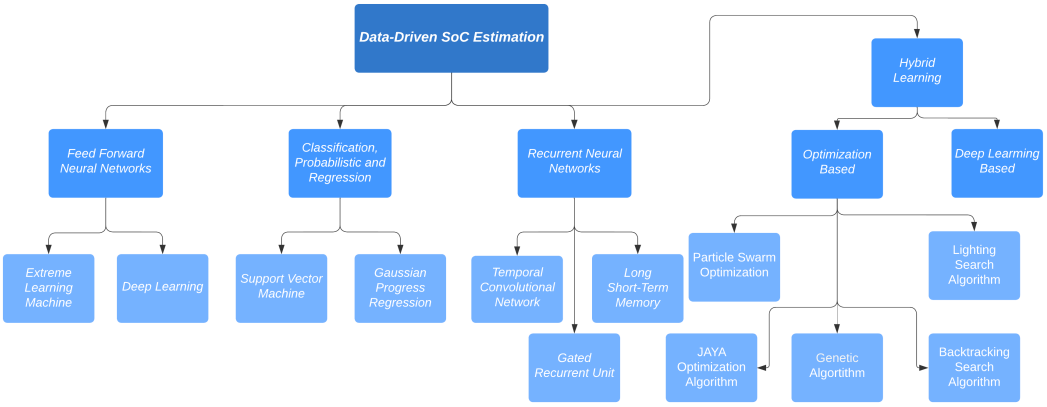

Figure 3: Illustration of different data-driven methods categorized [19].

A data-driven SOC estimation method involves two steps. The data-driven algorithm is first trained with data and then validated with before unseen data. Various types of data can be used for training and testing e.g. EV drive cycle data [21]. Advancement of cloud computing enables usage of a big data platform where multiple batteries can be monitored in real-time. The benefit of a big data platform is the abundance of data that covers different kinds of operating conditions instead of being limited into one device's data [18]. Another benefit is the available computational power. In addition to using real life data, Eleftheriadis *et al.* used data acquired from an electrochemical model, that is computationally too complex to be run in real-time, to train a neural network [19].

According to Wang *et al.*, a black-box model based SOC estimation method can be accurate but it may be restricted because it lacks actual behaviors and relationships of battery dynamics and does not consider other factors that affect the estimate like aging [18]. A study by Hossain Lipu *et al.* says that the other challenges are related to data abundance and data variety with data-driven methods. The accuracy of black-box models depends on the quality and amount of the available data. Because of it, there needs to be a large amount of varied quality data. This also causes the model to be sensitive to bad measurements, which can ruin the data. The collection of vast amounts of quality data that has sufficient variety can be difficult and time consuming, which can hinder the usage of black-box models in practical applications. In addition, the parameter and model structure selection is a process of trial and error, slowing the process even further [21].

2.3 Dynamic model based estimation

Compared with the black-box model based SOC estimation approaches, dynamic model based estimation methods require a knowledge of LiBs' internal dynamics. Modeling of

a LiB has few challenges. LiBs are time variant and non-linear with their impedance varying as a function of current, temperature and age [22]. Dynamic models can be divided into two categories, EMs and ECMs. The ECMs can be further divided into time-domain based and frequency-domain based models. The difference between these two is that the time-domain based models are identified from time-domain data and the frequency-domain based models are identified from a battery's frequency response data, which is called electrochemical impedance spectroscopy (EIS) [16]. The time-domain and frequency-domain models are not used for SOC estimation only by themselves but are coupled with a state estimator [9], [11].

2.3.1 Electrochemical models

EMs describe the electrochemical processes inside a battery by using thermodynamics and electrochemical kinetics [1]. The Doyle-Fuller-Newman (DFN) model is a first-principles electrochemical model for lithium-ion cells. The model has a group of coupled partial differential equations that describe a LiB cell behavior [11]. In literature, the DFN is also known as the pseudo two-dimensional model. Although the DFN model can fully describe the physical-electrochemical reaction inside a battery, the model is computationally too heavy for a real-time use and the partial differential equations might not even be convergent [23]. The DFN model relies on parameters that are impractical to identify and measure during operation [11].

Simplifications for the DFN have been made e.g. the one-dimensional model and the single particle model [1], [11]. From the simplified models, a state-space implementation of EM [23] and a simplified model with compensation for the simplified model's uncertainties [24] have been tested in a laboratory for real-time use.

2.3.2 Time-domain based

The measurable terminal voltage U_{int} changes with the current and temperature of a battery because the battery's impedance and OCV are functions of the current, temperature and battery's age. The terminal voltage cannot be directly used to estimate SOC unless the battery has reached the equilibrium state [11]. To get around this issue a ECM can be formed for the battery to calculate the open circuit voltage from the measured terminal voltage and current [7].

The simplest ECM is R_{int} model that only contains one resistor in series with the voltage source, Figure 4.

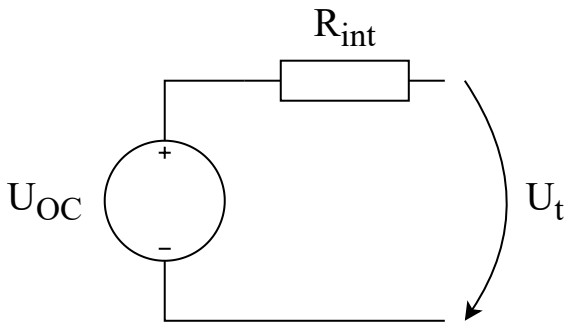

Figure 4: R_{int} equivalent circuit. U_{OC} is the open-circuit voltage.

In reality, a simple resistor does not capture the dynamics of batteries like it is illustrated in Figure 5 [11].

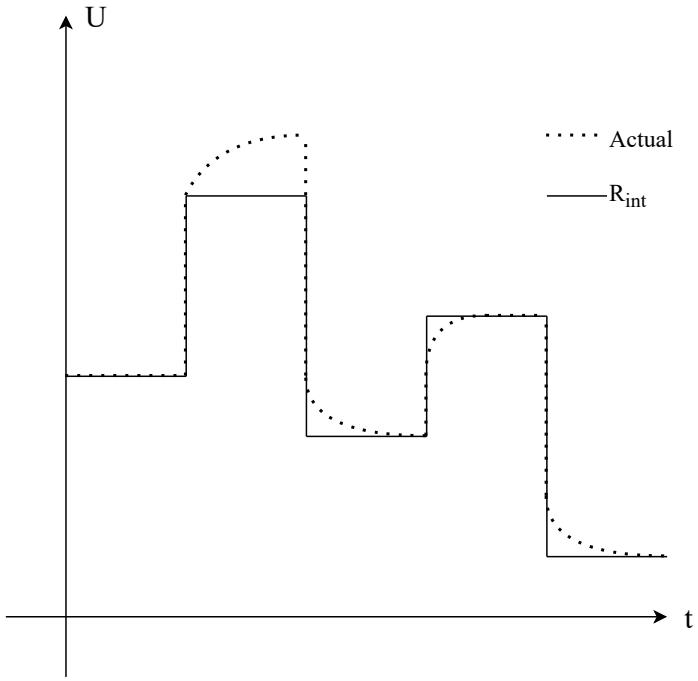

Figure 5: An illustration of actual battery voltage and R_{int} model voltage [11].

A more accurate model can be constructed by using a RC circuit. The RC circuit, Figure 6, can capture the dynamics of a battery. A arbitrary number of RC circuits can be added to series to add more time constants and potentially improve the accuracy of the model with the cost of adding complexity [11]. In literature the first-order RC circuit is often called Thevenin equivalent circuit and the second order dual polarization model.

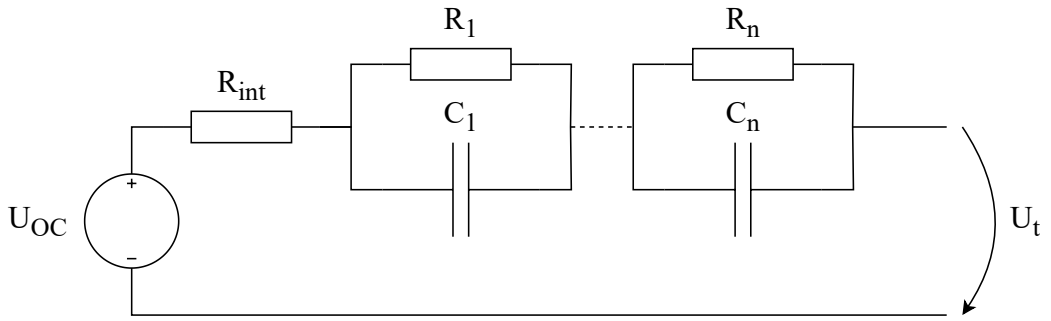

Figure 6: Nth order RC circuit.

Studies by Hu *et al.*, Lai *et al.* suggest that while the second-order RC is more accurate than the first-order, it is not significantly more accurate to justify the increased complexity in parameter identification and computational cost [25], [26]. Case studies by Shen and Xiong also suggest that the first-order RC is the best choice [1]. Study by Zhao *et al.* claims that the second-order is better for its accuracy since the maximum difference in the error of SOC estimate with the first and second-order RC circuits is about 4 % [27]. Having more than two RC components can cause overfitting issues and make the model more susceptible to measurement noise [25], [28]. According to Hu *et al.* LFP benefits from adding hysteresis to the model and increasing its accuracy, while both Hu *et al.*, Lai *et al.* say that NMC model's accuracy suffers [25], [26]. Moreover, the first-order RC circuit is the most suitable if identifying parameters online [1], [29].

In addition to the RC model, other ECMs have been proposed. One such is a more complex model proposed by Biju and Fang that has equivalent circuits approximating chemical reactions of electrochemical models [30].

Other model that comes across in literature is the partnership for a new generation of vehicle (PNGV) circuit, Figure 7.

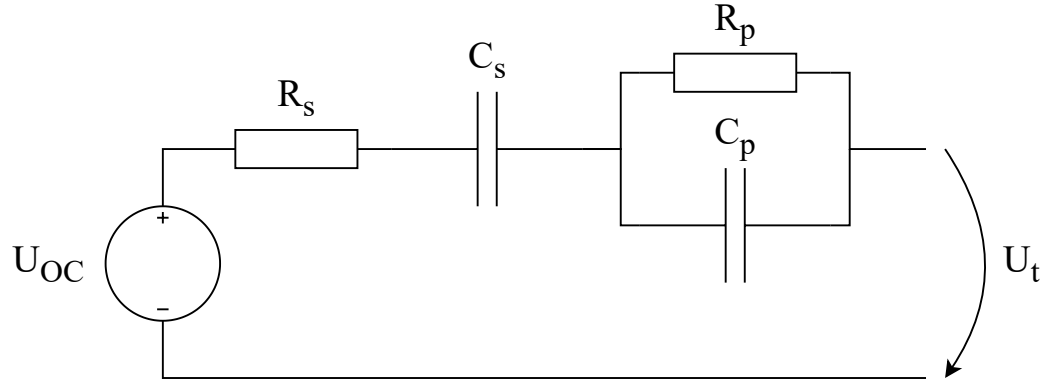

Figure 7: PNGV circuit.

The difference between the RC and PNGV model is that the PNGV includes a series capacitor in addition to a resistor. The PNGV is less complex than the second-order RC circuit and models low SOC (0 % - 20 %) better than the RC circuit [29].

In addition to continuous-time ECM models, there are discrete-time time-series models. A auto-regressive model with exogenous input (ARX) can be used to model a LiB. The ARX is presented in Figure 8. The benefit of the ARX model is that it is a discrete model since continuous models need discretization to be used programmatically. According to the Yuan *et al.*, the second-order ARX model is the best compromise between accuracy and computational efficiency [31], [32].

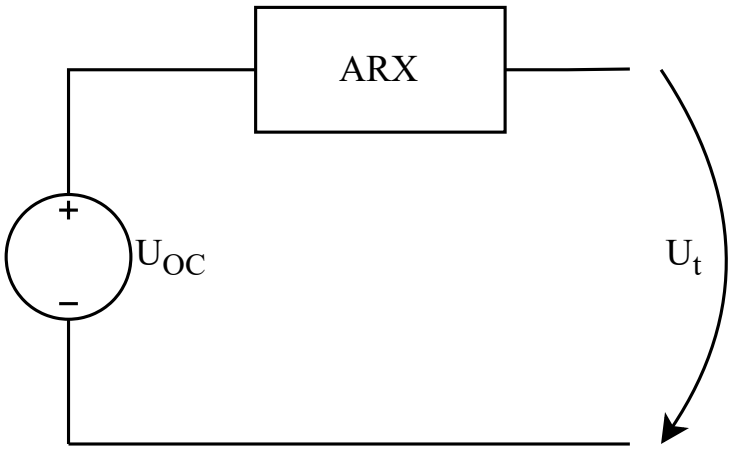

Figure 8: Arx model.

The time-domain based models' parameters can be identified either online or offline. The offline identification is based on selecting the desired model and fitting the parameters to previously acquired battery voltage, current and temperature data that can be acquired e.g. from the hybrid pulse power characterization (HPPC) [33]. In the HPPC a charge pulse is first applied and then a discharge pulse. Fitting is often done using a least-squares method, genetic or particle swarm optimization algorithm [1], [9]. There are also other methods such as the pulse charge and the pulse discharge test where the batteries' relaxation curve is measured and time constants are approximated from the transient [16]. In addition to the HPPC, other types of excitations for batteries have been introduced such as the Urban Dynamometer Driving Schedule [34].

The online identification works by identifying a model in real-time as a vehicle is in use. The online identification usually uses a modified least-squares algorithm e.g. the recursive least-squares. While the offline identification provides a more accurate results, the online identification can be also used supplementally to improve the model parameters while in use since batteries are time variant [1]. The most suitable algorithm for the model parameter identification depends on the battery type and the model type [29].

2.3.3 Frequency-domain based

Frequency-domain models are based on batteries' frequency response, the so called EIS, which was first proposed in 1985 [10]. The frequency-domain ECMs are identified from a LiB's frequency response. A study by Xu *et al.* suggests that a frequency-domain model is more accurate than a time-domain RC model [35]. In addition to using the EIS to parameterize a ECM, it has also been tested for direct SOC estimation. It has been found that SOC and a LiB's impedance have a monotonic relationship but there is a practical limitation, the SOC needs to be updated regularly and the battery needs to be in steady-state to measure the frequency response [36]. Figure 9 illustrates a typical EIS measurement results in Nyquist diagram [11].

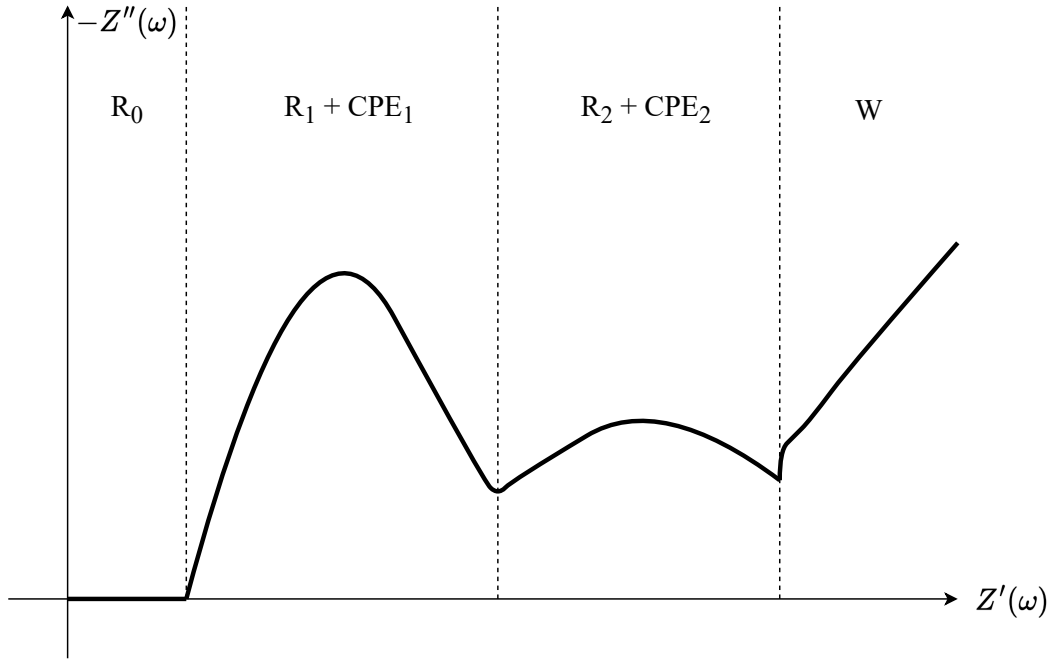

Figure 9: A typical EIS Nyquist plot for LiB [11].

The measured EIS can be interpreted as a equivalent circuit. The ECMs interpreted from the EIS are called fractional order models. Fractional order models are equivalent circuits where capacitors are replaced with constant phase elements (CPEs). In addition to the CPEs, Warburg element is also added to the circuit [9]. Figure 10 is a fractional order circuit interpreted from the Nyquist diagram presented in Figure 9.

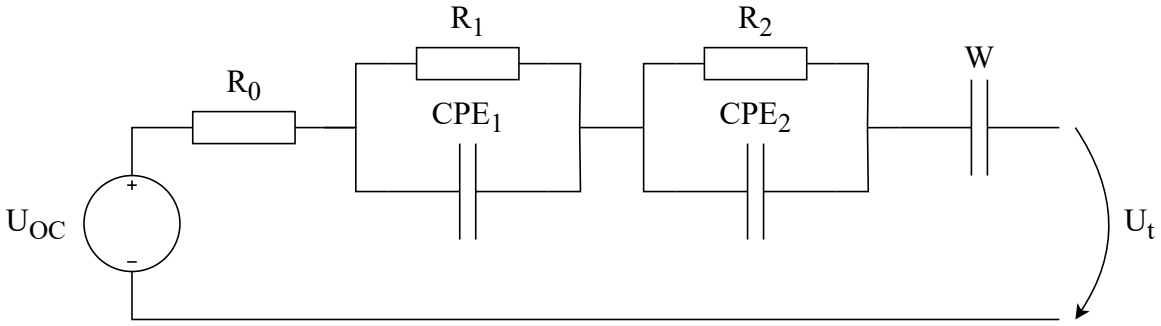

Figure 10: Fractional order circuit. W component is the Warburg element [11].

R_0 is the Ohmic resistance of a cell. R_1 + CPE_1 is caused by the effects of solid electrolyte interface (SEI). R_2 + CPE_2 represents the double layer effects and charge transfer resistance at the electrodes [37]. The parallel of a resistor and a CPE is called Zarc element [38]. CPE is defined as shown in Equation 2.2

$$Z_{CPE} = \frac{1}{(j\omega)^n \theta} \; n \in [0, 1] \tag{2.2}$$

where n is the depression factor of the semi-circle in the Nyquist diagram and θ is the generalized capacity. For $n = 0$ it is resistance only element, for $n = 1$ it is equal to capacitor, Figure 11. If $n = 0$, the Zarc and RC circuit equations are equal [38].

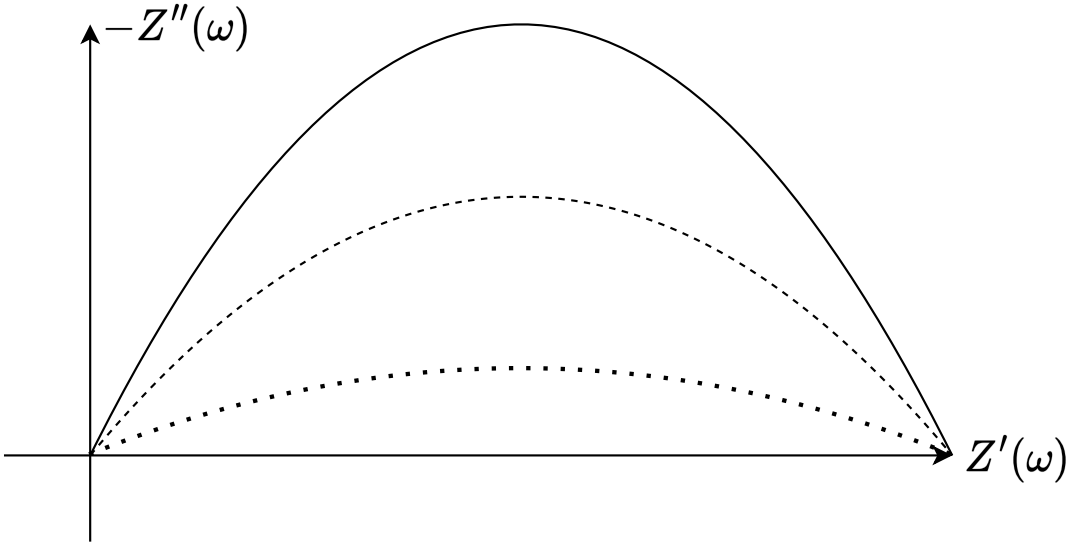

Figure 11: Illustration of Zarc as n gets smaller. Highest n at solid line and smallest at dotted line with dashed line in-between [11].

In addition to the Zarc element, fractional order models also include the Warburg element [38]. The Warburg element is just CPE with $n = 0.5$ and has constant phase shift of 45°[11].

The Warburg element emulates the diffusion processes in the electrode at low frequencies [37].

The benefit of the Zarc elements is the ability to produce depressed semi-circles in the frequency-domain, which are characteristic of a lithium-ion cell. The disadvantage of the Zarc and Warburg elements is that there is no Laplace transform, thus approximations are required. One way to approximate Zarcs is to use RC-elements. Increasing the order of RC circuits increases the accuracy of the approximation but it also increases the computational load. To approximate the Warburg element, one serial resistor and RC circuit works [38], [39]. Digital filters can be also used to approximate the Zarc and Warburg elements [11].

The EIS measurement is done to a cell by using current excitation. Typically EIS measurements are made at low currents. For systems with higher rates, the EIS currents should be higher to obtain more relevant parameters for high current use [11]. If measuring battery impedance in a pack then a battery's cells should be balanced and temperature should be equal among them [36].

The EIS is limited in its use for online applications due to the special current waveforms required, thus the EIS is more useful for initial parameter identification with online methods for parameter updates. There are multiple excitation signal types, Figure 12.

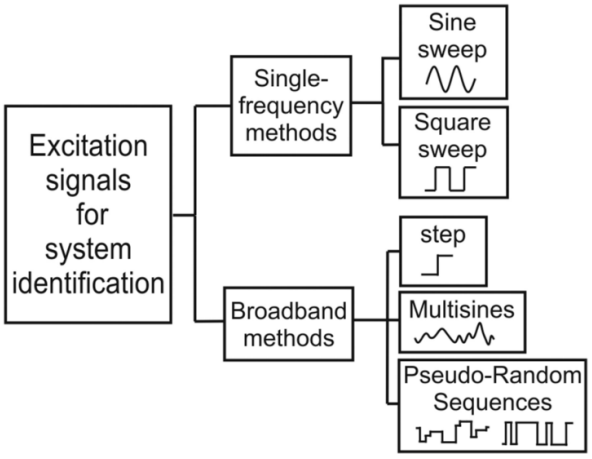

Figure 12: Different types of excitation signals [40].

Traditionally the response is excited with a sinusoidal sweep because of its accuracy but it is both slow and complex, which makes it hard for online use. Cycle times up to hours are not uncommon. Broadband excitation methods are used to counter the slowness of the sinusoidal sweep but they come with their own drawbacks e.g. worse signal-to-noise ratio (SNR) [11], [40].

2.3.4 State estimators

State estimators like the Luenberger estimator, sliding mode observer, PI observer, H_∞ filter and Kalman filter are used with ECMs to estimate the SOC [1]. Feedback methods are the only difference between the mentioned state estimator techniques and the structure of the methods can be generalized into a form that is shown in Figure 13. From control theory view, these different estimation methods can be considered as a control loop. While a controller tries to reduce the error between the system input and output, a state estimator tries to reduce the error between model's output and real system's output [41].

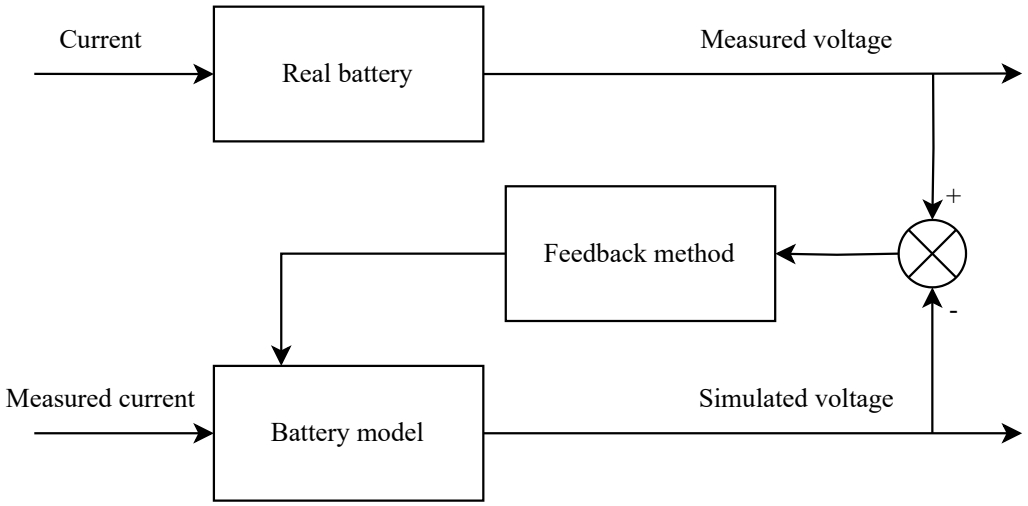

Figure 13: Typical state estimator SOC estimation loop [41].

The Luenberger estimator for SOC estimation takes the error of a battery model's output voltage and the battery's terminal voltage and applies a gain that has to be tuned for the estimator. The Luenberger is common for its simplicity and the ease of tuning but it is accurate only for deterministic and linear systems. Compared to the Kalman filters (KFs), it has poorer accuracy in SOC estimation since measurements cause stochastic noise and LiBs are non-linear. Improvements to the Luenberger's accuracy have been proposed such as a adaptive Luenberger estimator [42], [43].

The PI observer applies integrator in addition to the gain into the voltage estimation error, which makes it more robust to modeling errors. PI observer is akin to a PI controller, allowing it to be tuned like one. It is easy to implement and it has been shown to be accurate for linear and non-linear system state estimation [41].

In addition to the Luenberger estimator and PI observer, the sliding mode observer and H_∞ filter have also shown to be working in SOC estimation [44], [45].

The KF is a optimal state estimator [46]. The KFs were first introduced to SOC estimation in 2000 [10]. It is the most used state estimator for SOC estimation [47]. The KF expects

noise to be white, Gaussian and having zero mean. In most situations, the used model is an approximation of the true battery dynamics and deviations in the model from a actual battery are deterministic, therefore the errors are not strictly random in nature. It is also impossible to say that the error components are always Gaussian. Despite these, the KFs have been shown to be reliable in estimating SOC [11]. Though other observers are computationally less expensive than KFs [9].

The KF updates the Kalman gain online based on the error covariance matrices [48]. The steady-state Kalman filter (SSKF) uses the Riccati equation to solve the Kalman gain beforehand, reducing the computational overhead while online [49]. On the downside it cannot be used with online model parameter estimation because the Kalman gain depends on state matrices in a state-space model, unless the Riccati equation is used again to compute the Kalman gain using the updated state-space model [34], [50], [51].

A non-linear KF is used when estimating a battery SOC because the OCV-SOC relationship is not linear. The non-linear KFs are extended Kalman filter (EKF), central difference Kalman filter (CDKF), unscented Kalman filter (UKF) and cubature Kalman filter (CKF), Figure 14 [47]. A case study done by Shen and Xiong comparing the EKF and H_∞ filter found out that the EKF is slightly more accurate than the H_∞ filter [1].

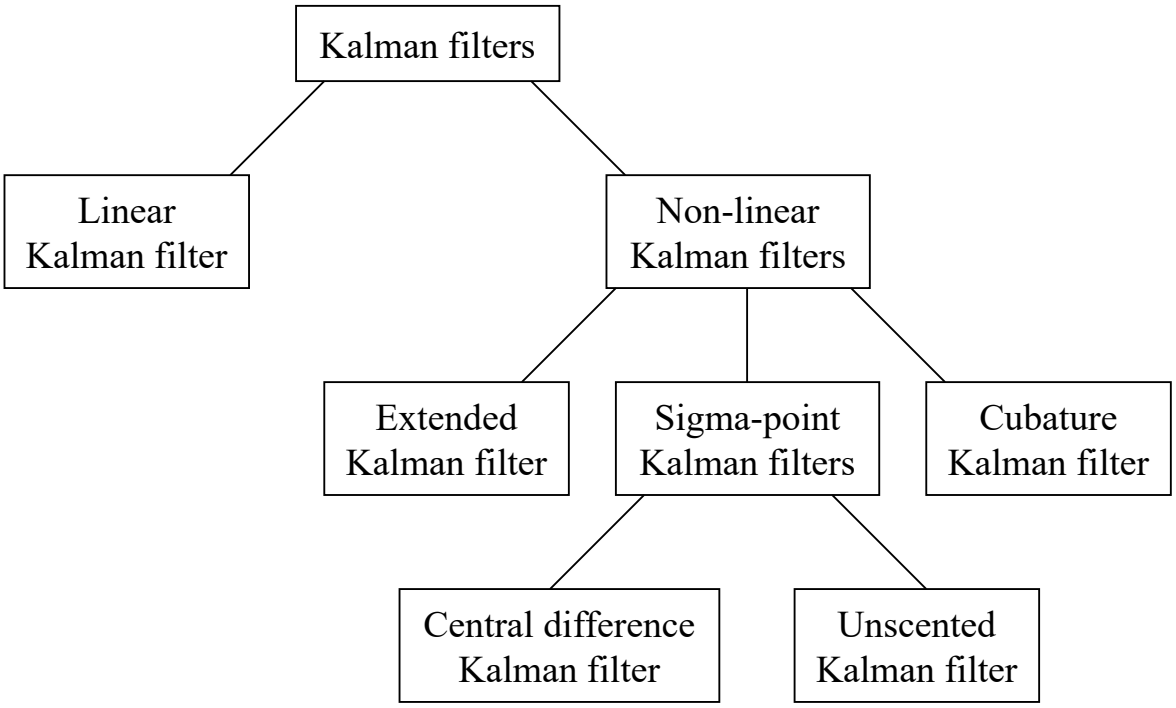

Figure 14: Kalman filter family tree [47].

The EKF requires computation of the Jacobian matrix, a matrix of partial derivatives. The derivative of the SOC-OCV relationship is required, as well as the derivative of model parameters in respect to the state-space model's states. Computing this in real-time is com-

putationally taxing but the partial derivatives can be formulated beforehand and be used as look-up table to lessen the computational burden [11], [46]. In addition to being computationally expensive, the EKF includes modeling error since the process linearizes the non-linear functions [18]. According to a study done by Shrivastava *et al.* the SOC estimation mean absolute error (MAE) with the EKF is less than 4 % [47].

Another technique is the UKF, which avoids the calculation of the Jacobian. The UKF gets sampling points that it uses for approximation, thus avoiding problems caused by the linearization, being computationally more efficient and more accurate [9], [47]. With the UKF, the SOC estimate MAE is less than 2 % [47]. Although it has these benefits over the EKF, it has some drawbacks. If the initial state guess is far from the actual value, the estimation accuracy decreases and divergence increases. The estimate might not even converge at all [18]. It is also susceptible to measurement noise as it increases divergence, thus increasing computation time [47]. The UKF is a so called sigma-point Kalman filter as the sampling points are called sigma-points.

Another sigma-point Kalman filter is the CDKF. The CDKF works on the same principle as the UKF but the weighing factor differs, as there is only one parameter to tune with the CDKF. The CDKF is simpler to implement than the UKF because of the only one tuneable parameter, and in theory it is also more accurate [50]. Computationally it is more complex than the UKF with a higher order state matrix. In literature, the CDKF has been shown to be accurate with MAE of less than 0.6 %, while both the UKF and the CDKF show increased speed and accuracy over the EKF [47].

The CKF was introduced to address the convergence problems of the sigma-point KFs. It shows higher accuracy with MAE of less than 0.5 %, better stability and is less complex than the EKF and the UKF [18], [47]. On the downside it has longer convergence time than the EKF. Improvement to the CKF has been proposed with the adaptive CKF that has lower convergence time than the EKF and the UKF [47], [52].

2.3.5 Pack modeling

A single cell cannot meet the requirements of EV use, thus batteries come in packs where there are multiple cells in series and parallel. Estimating the SOC for each cell takes computing resources. For a series of cells, two types of simplifications have been proposed. The first one of these is a big cell approach where the whole pack is regarded as one big cell. Another method is cell mean method where an extreme or average cell is selected and it is used to describe the system. With either of these approaches, the typical SOC estimation methods can be used. The downside is that cells cannot be balanced [7], [53], [54].

Parallel cells are often considered to be acting like a single cell with an assumption that a current is equally distributed among them [55]. The mean cell method has been used for parallel cells [54], [56]. Each cell can be estimated individually with Kirchoff's laws [55], [57]. For the big cell model, characterization of LiB packs can be done on a whole pack instead of having to individually characterize each cell [42], [58].

3 IMPLEMENTATION OF SOC ESTIMATION

The best fit for our use case would be just the Coulomb counting because of its simplicity. Because of its drawbacks, it cannot be used on its own. A SOC-OCV function would be also a good option but it cannot be used with LFP batteries or while the battery is under a load.

The EIS cannot be used on a ship to form a battery model because there could be more than tens of meters of cable between the excitation source and the battery, which affects the excitation signal. The inverter units used include inductance at the output, which affects the excitation signal in addition to the cable, and the inverters themselves do not support excitation required for the EIS.

Data-driven estimation methods are not suitable either because training them requires a large amount of data that we do not have. EMs are computationally too heavy to be run while a ship is running and require information that needs to be acquired in laboratory conditions.

The time-domain based models are the best fit because in addition to being able to do the tests required for parameterizing one, they can be also used while under a load. The ARX model is selected because it is directly a discrete model, thus it is straightforward to implement programmatically since a continuous-time ECM requires discretization for it to be implemented. To parameterize the ARX model, data for the system identification is required. The HPPC sequence is used to acquire data from which to parameterize the model. The least-squares algorithm is used to parameterize the model. The ARX model also allows for a online parameter identification method to be implemented in the future to take into account the aging of the battery. Using the ARX with the linear KF and the EKF is simple because the ARX is linear, thus it requires no linearization. The second-order ARX model is used because it offers good accuracy with smaller computing overhead than the higher order ARX models. No hysteresis is included in the model because literature suggests that adding hysteresis to NMC cell's model decreases its accuracy.

In addition the model based SOC estimation requires the OCV-SOC relationship to be characterized. The Coulomb counting is also implemented into the model.

Usually batteries in marine applications are not individual cells but packs, which needs to be taken into account when modeling a battery system. In our use, the big cell approach is natural choice since cell balancing is not an issue because the battery management system (BMS) takes care of that. In addition, we do not always have access to the individual cell data or ability to characterize the individual cells. But because we only have one cell for

measurements at this time, the pack modeling does not need to be taken into account in the implementation.

When estimating the SOC from the model, a state estimator is used. The SSKF is used because of the limitations with PLC's runtime environment. The runtime environment does not support matrix operations by itself, thus implementing a other type of KF would also require implementing a linear algebra library that supports e.g. Cholesky factorization and inversing matrices, which is not in the scope of this thesis. The SSKF only requires matrix multiplication and summing, which can be implemented with for-loops. The downside of the SSKF is that the model cannot updated online unless the Kalman gain is computed again using the new model parameters. In addition to the SSKF, the EKF is also implemented to compare the error rate between a linear model and a non-linear model and as a future-proof in case the marine team ever decides to move from PLCs to industrial PCs.

3.1 Estimator loop

The whole SOC estimation system is encapsulated in Figure 15.

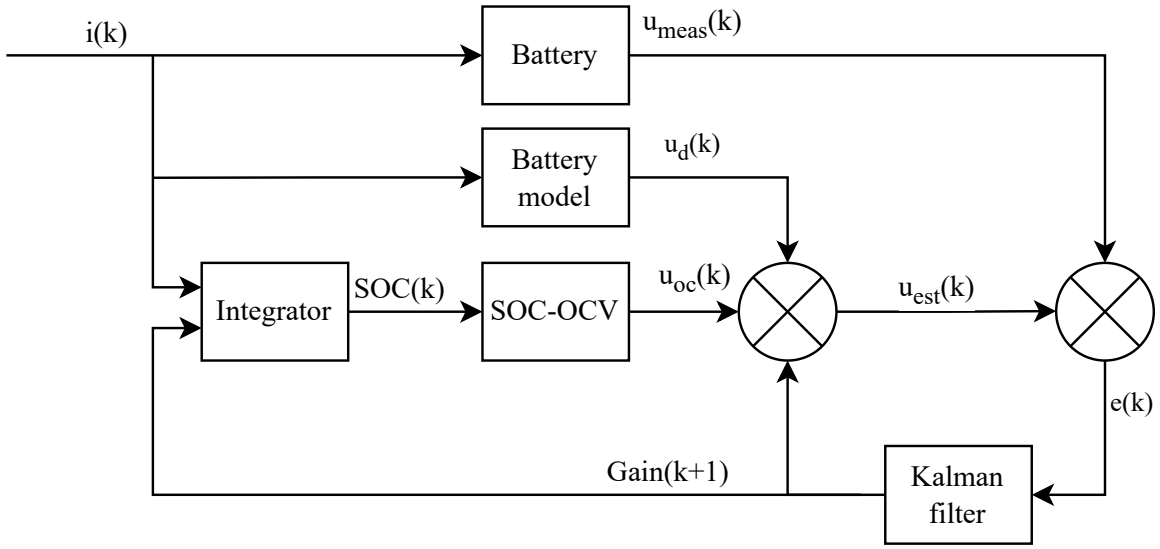

Figure 15: Estimator loop.

The current and terminal voltage of the battery are measured and inserted into the estimator loop. The current is then given to the battery model and the integrator. The integrator integrates current over time and outputs a SOC estimate. The SOC estimate is then given to the SOC-OCV function. The function outputs the OCV based on the the SOC estimate. The battery model outputs dynamic component of the voltage of the battery. The OCV and dynamic voltage are summed with the output being terminal voltage estimate. The terminal voltage estimate is then compared to the measured terminal voltage and the error is multiplied by the Kalman gain that is then added to the state equation on the next iteration.

The second-order ARX model in generic form without any added input delays is in Equation 3.1

$$y(k) + a_1 y(k-1) + a_2 y(k-2) = b_0 x(k) + b_1 x(k-1) \tag{3.1}$$

where $y(k)$ is the model's output at time k, $x(k)$ is the input at time k, a_i is the output parameter and b_i is the input parameter. The ARX model is parameterized with MATLAB's `arx` function [59].

To estimate the SOC, the ARX model needs to be augmented with a SOC-OCV function and current integrator for the Coulomb counting. Linear function, Equation 3.2, is fitted into the data since the SSKF can only handle linear systems

$$u_{OCV}(SOC) = a_{ocv}\, SOC(k) + b_{ocv} \tag{3.2}$$

where SOC is the SOC estimate at time k, a_{ocv} is the slope and b_{ocv} is the intercept of the linear equation.

The current integrator from Equation 2.1 in discrete form is in Equation 3.3

$$SOC(k) = \frac{\eta T_s}{Q_{max}} i(k) + SOC(k-1) \tag{3.3}$$

where $i(k)$ is the current at time k, η is the Coulombic efficiency when charging, T_s is the sample time when it is constant, and Q_{max} is the maximum capacity.

The ARX model is transformed into state-space model. A generic discrete state-space model is in Equation 3.4

$$\begin{cases} x(k) = Ax(k-1) + Bu(k) \\ y(k) = Cx(k) + Du(k) \end{cases} \tag{3.4}$$

where A is the system matrix, B is the input matrix, C is the measurement matrix, D is the feedthrough matrix, $x(k)$ is the state vector at time (k) and $u(k)$ is the input vector at time (k). It is augmented with the current integrator and the SOC-OCV function. The augmented state-space model is presented in Equation 3.5 when the ARX model order is two

$$\begin{cases} \begin{bmatrix} u_d(k) \\ u_d(k-1) \\ SOC(k) \end{bmatrix} = \begin{bmatrix} -a_1 & -a_2 & 0 \\ 1 & 0 & 0 \\ 0 & 0 & 1 \end{bmatrix} \begin{bmatrix} u_d(k-1) \\ u_d(k-2) \\ SOC(k-1) \end{bmatrix} + \begin{bmatrix} b_0 & b_1 \\ 0 & 0 \\ \frac{\eta T_s}{Q_{max}} & 0 \end{bmatrix} \begin{bmatrix} i(k) \\ i(k-1) \end{bmatrix} \\ u_{est} = \begin{bmatrix} 1 & 0 & OCV(SOC) \end{bmatrix} \begin{bmatrix} u_d(k) \\ u_d(k-1) \\ SOC(k) \end{bmatrix} \end{cases} \tag{3.5}$$

where $u_d(k)$ is the dynamic voltage at time k and $u_{est}(k)$ is the estimated voltage at time k and $OCV(SOC)$ is the SOC-OCV function. For the state-space model, the Kalman gain is computed by MATLAB's `dlqr` function [60]. The model's equation with the Kalman gain for the SSKF and the linear SOC-OCV function is Equation 3.6

$$\begin{cases} \begin{bmatrix} u_d(k) \\ u_d(k-1) \\ SOC(k) \end{bmatrix} = \begin{bmatrix} -a_1 & -a_2 & 0 \\ 1 & 0 & 0 \\ 0 & 0 & 1 \end{bmatrix} \begin{bmatrix} u_d(k-1) \\ u_d(k-2) \\ SOC(k-1) \end{bmatrix} \\ \qquad + \begin{bmatrix} b_0 & b_1 \\ 0 & 0 \\ \frac{\eta T_s}{Q_{max}} & 0 \end{bmatrix} \begin{bmatrix} i(k) \\ i(k-1) \end{bmatrix} + \begin{bmatrix} L_1 \\ L_2 \\ L_3 \end{bmatrix} (u_{meas}(k-1) - u_{est}(k-1)) \\ u_{est}(k) = \begin{bmatrix} 1 & 0 & a_{ocv} \end{bmatrix} \begin{bmatrix} u_d(k) \\ u_d(k-1) \\ SOC(k) \end{bmatrix} + b_{ocv} \end{cases} \tag{3.6}$$

where $u_{meas}(k)$ is the measured terminal voltage of the battery at time k and L_i is the Kalman gain.

The EKF model is quite similar to the SSKF model with the difference being that the SOC-OCV function is not linear and the Kalman gain is time-variant. The EKF works by linearizing the non-linear function at the values of estimated states, which yields linear functions placed at the estimates. In practice, a higher order polynomial for the SOC-OCV relationship is parameterized and it is then derivated. It is partially derivated in respect to every state

of the state-space model. Almost every partial derivation yields zero expect for derivation in respect to the SOC since the only variable in the function is the SOC. From the derivated function the value of the derivative at every SOC can be computed. The value of the derivative is the slope of a linear function placed at that point. After that, the intercept for the linear function is computed. The acquired linear equation is then used in the model for the SOC estimation. This process is repeated at every timestep. The partial derivative of the SOC-OCV function can be calculated analytically beforehand reducing the computing overhead. The modified model for the EKF is presented in Equation 3.7

$$\begin{cases} \begin{bmatrix} u_d(k) \\ u_d(k-1) \\ SOC(k) \end{bmatrix} = \begin{bmatrix} -a_1 & -a_2 & 0 \\ 1 & 0 & 0 \\ 0 & 0 & 1 \end{bmatrix} \begin{bmatrix} u_d(k-1) \\ u_d(k-2) \\ SOC(k-1) \end{bmatrix} \\ \qquad\qquad + \begin{bmatrix} b_0 & b_1 \\ 0 & 0 \\ \frac{\eta T_s}{Q_{max}} & 0 \end{bmatrix} \begin{bmatrix} i(k) \\ i(k-1) \end{bmatrix} + \begin{bmatrix} L_1(k) \\ L_2(k) \\ L_3(k) \end{bmatrix} (u_{meas}(k-1) - u_{est}(k-1)) \\ \\ u_{est}(k) = \begin{bmatrix} 1 & 0 & \frac{\delta OCV}{\delta SOC} \end{bmatrix} \begin{bmatrix} u_d(k) \\ u_d(k-1) \\ SOC(k) \end{bmatrix} + y_{intercept} \end{cases} \tag{3.7}$$

where $\frac{\delta OCV}{\delta SOC}$ is the slope of the SOC-OCV function at SOC, $y_{intercept}$ is the intercept of the linearized function and $L_i(k)$ is Kalman gain at time k.

The EKF requires computation of the Kalman gain online, Equation 3.8

$$\begin{cases} P_{cov}(k) = AP_{cov}(k)A^\intercal + Q \\ L(k) = P_{cov}(k)C^\intercal(CP_{cov}(k)C^\intercal + R)^{-1} \\ P_{cov}(k+1) = P_{cov}(k) - L(k)CP_{cov}(k) \end{cases} \tag{3.8}$$

where $P_{cov}(k)$ is error covariance at time k, $L(k)$ is the Kalman gain matrix at time k, Q is the process noise matrix, R is the measurement noise matrix. The P_{cov} value is initially guessed, it then iterates and converges based on the system matrices and the noise covariances.

4 MEASUREMENTS

The measurements are made on a KeepPower 18650 LiB that is a NMC cell, which has 3.5 Ah nominal capacity and 3.7 V nominal voltage, with a Neware battery testing system model CT-4008T-5V12A-S1. All of the measurements are made in room temperature while the building's ventilation system keeps the temperature constant. The OCV and the HPPC discharge tests are made on a different battery cell than the ferry load profile and the HPPC charge tests.

The first measurement is the capacity. The measurement is presented in Figure 16.

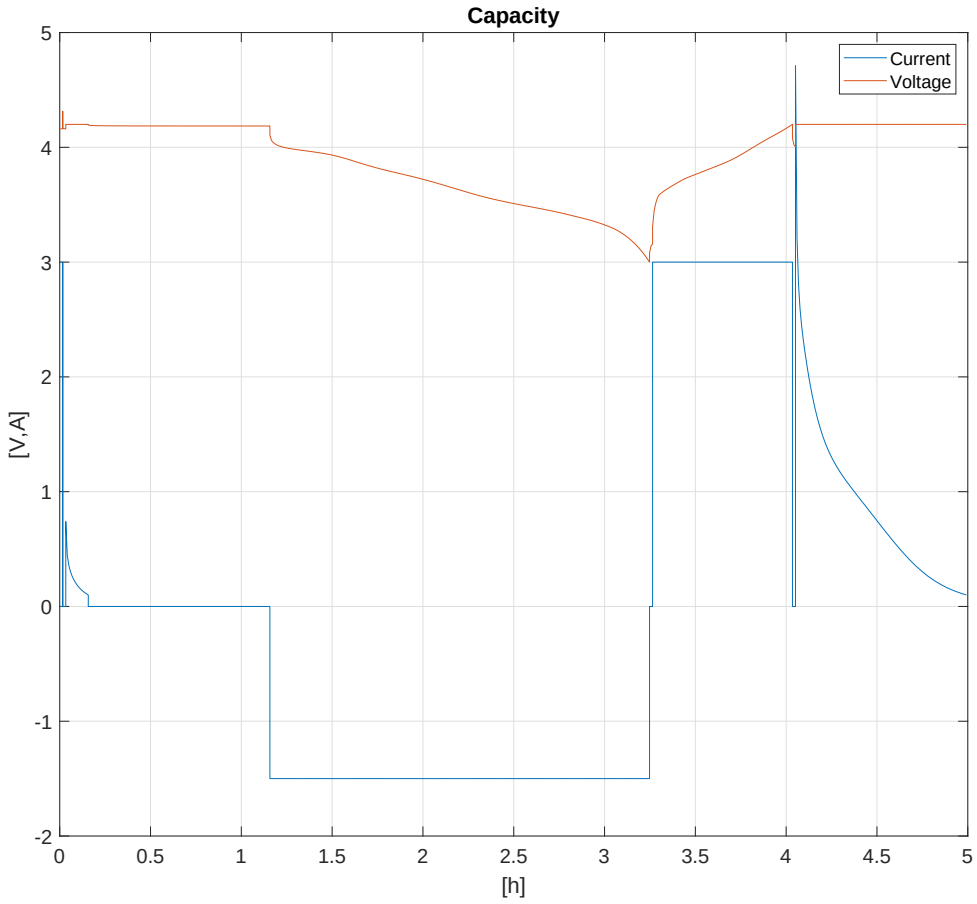

Figure 16: Capacity measurements.

The battery is first constant current (CC) charged to 4.2 V. Then it is constant voltage (CV) charged with a 100 mA cut-off current. It is then left to rest at 100 % SOC for an hour before it is discharged. The capacity is measured from one full discharge cycle at 1.5 A from 4.2 V

to 3.0 V. After the charging, it is recharged back to full with the same method as on the first charge. The measured capacity from the discharge is 3.1352 Ah. The measured capacity is used for the SOC adjustments in later measurements and for the max capacity in estimation.

The next one is OCV measurement. It is done to acquire the SOC-OCV function. The measurement is presented in Figure 17.

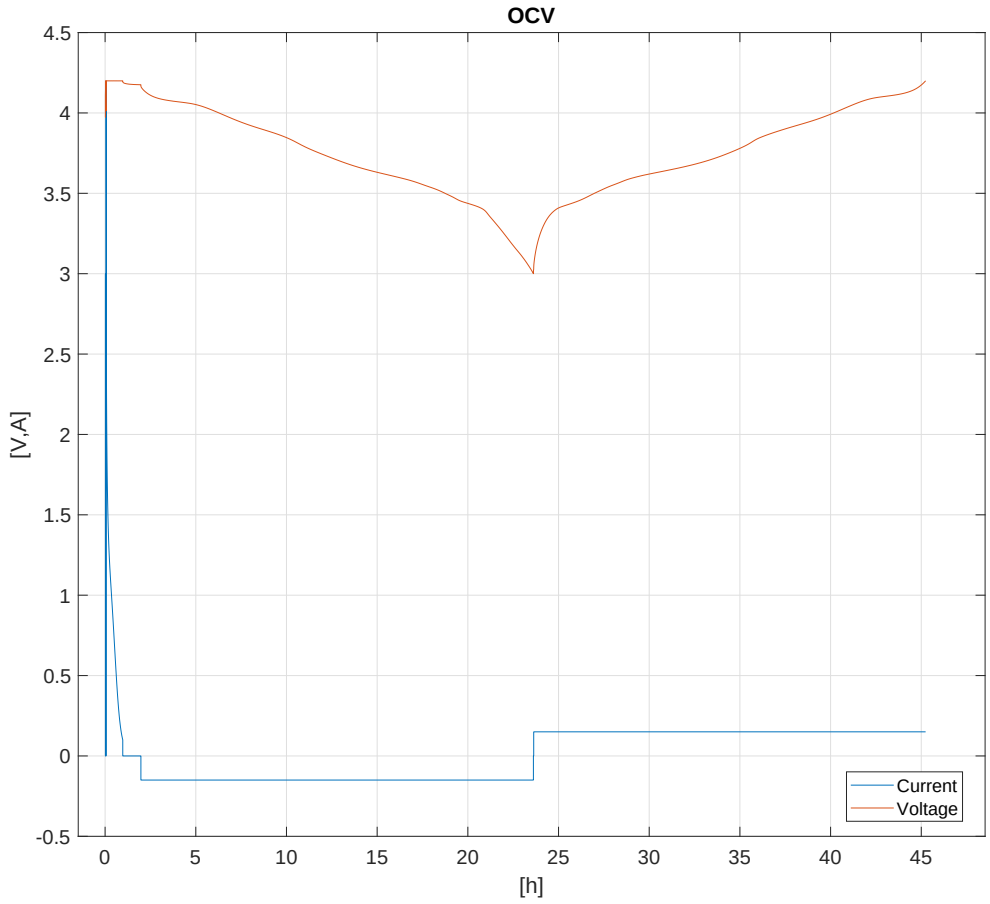

Figure 17: OCV measurements.

The battery is first CC-CV charged to 4.2 V with a 100 mA cut-off current. It is then left to rest at 100 % SOC for an hour before the measurement. The OCV is measured at 150 mA between 4.2 V and 3.0 V for both the discharging and charging. The discharge capacity is used as maximum charge for both the charging and discharging.

The HPPC measurements are done for both the charging and discharging. The discharge HPPC is used to parameterize the ARX model and the charge HPPC is for the estimator testing. The discharge HPPC is is Figure 18.

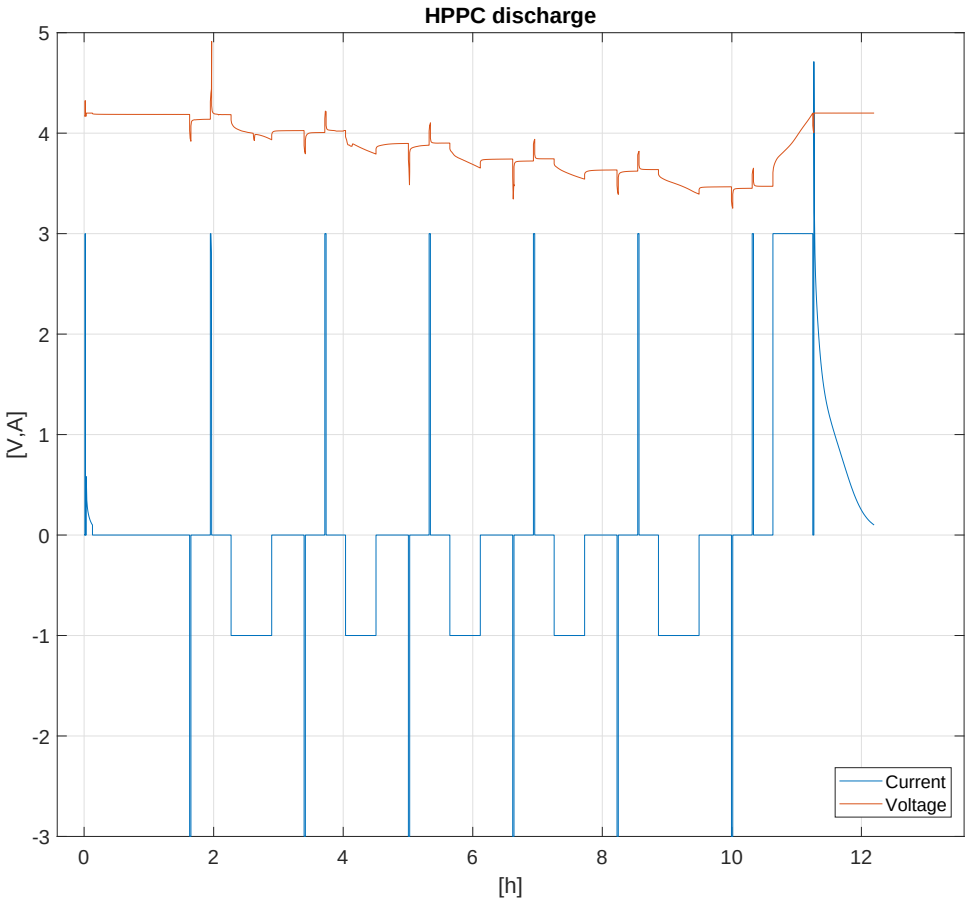

Figure 18: HPPC discharge measurements.

The battery is CC-CV charged to 4.2 V with 100 mA cut-off current and let to rest at 100 % SOC for an hour before the measurement is done. The HPPC pulse sequence first contains a 30 minute rest period at start, then 3 Ampere discharge for 72 seconds, 1080 second rest, 3 Ampere charge for 72 seconds and then 1080 second rest again. The HPPC measurements are repeated at 100 %, 80 %, 65 %, 50 %, 35 % and 15 % SOC. The first measurement is done at 100 % SOC. Then the SOC is adjusted to 80 % and the pulse sequence is repeated for each SOC until it is 15 % SOC.

The charge HPPC test for the estimator validation is ran on the battery. The measurement is in Figure 19.

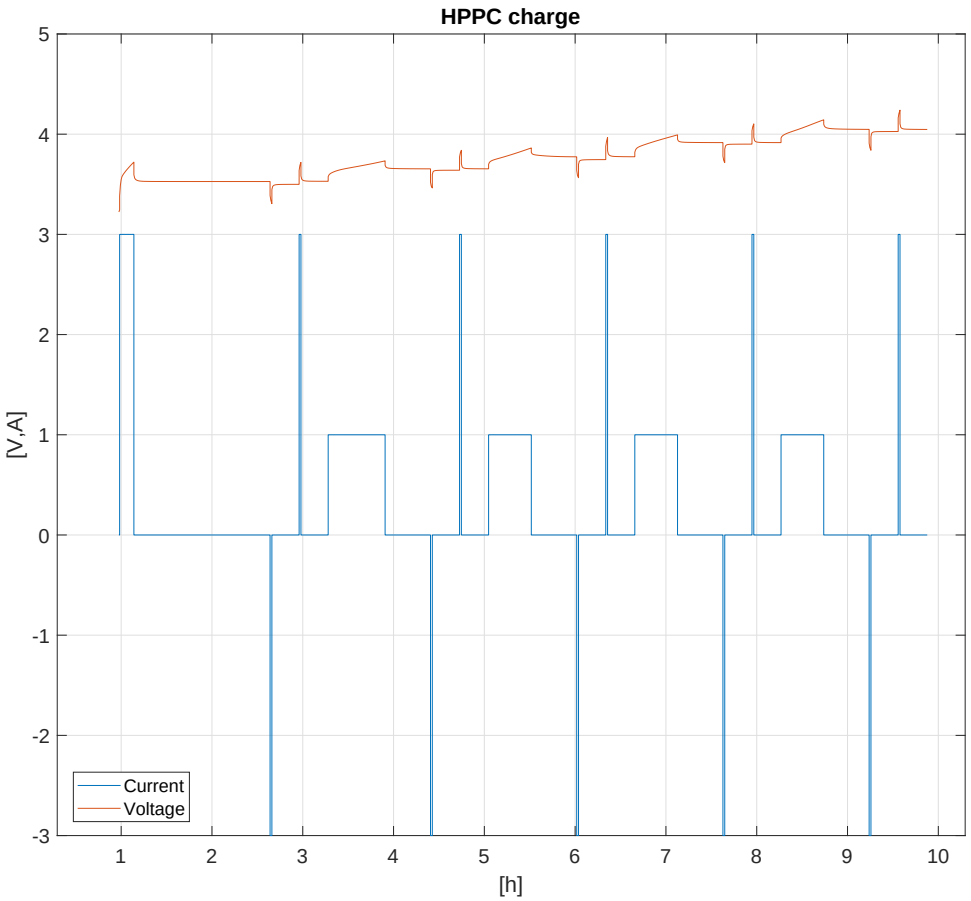

Figure 19: HPPC charge measurements.

The battery is first discharged to 3 V and it is then recharged to 15 % SOC where the HPPC pulsing is done using the same intervals as in the HPPC discharge. The HPPC measurements are repeated at 35 %, 50 %, 65 % and 80 % SOC.

Lastly, a ferry load profile is ran on the battery. The load profile is ran on the battery to acquire battery data that replicates it being used in a real ferry use to validate the SOC estimation. The load test is in Figure 20

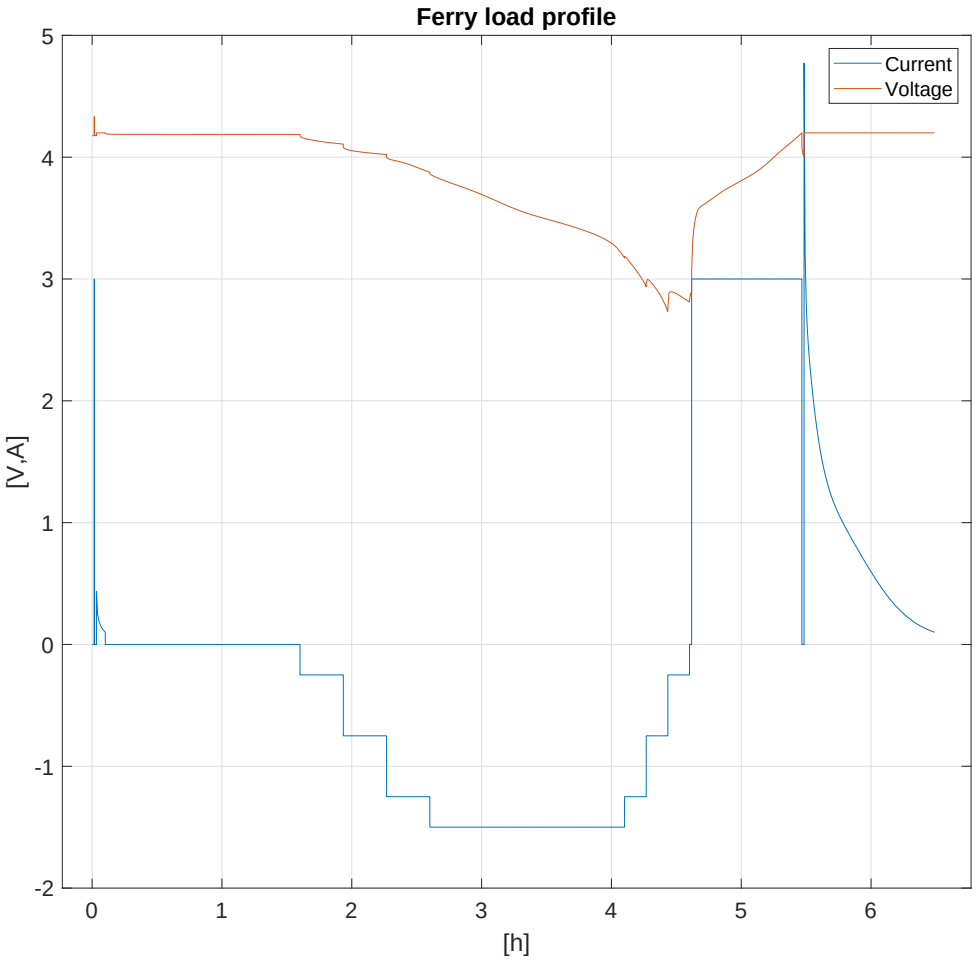

Figure 20: Load profile measurements.

First, the current is ramped in three 20 minute steps to 1.50 A with the steps being 0.25 A – 0.75 A – 1.25 A. The battery cycler has limited ramping capability and the ramping has to be done manually. Then, the constant current lasts for 2 hours where the battery is emptied. And lastly, the current is ramped to 0 A in three 10 minute steps using same amplitudes as in the upwards ramping. Afterwards it is CC-CV charged to full.

5 MODEL PARAMETERIZATION AND VALIDATION

The LiB model is parameterized and validated from the measurements. The battery cycler the measurements were made on has a base sample time of 30 seconds but it sometimes takes sporadic measurements and can include multiple measurements on the same timestep, thus the measurement data is processed before it is used for the ARX model parameterization and the estimator validation. First, multiple measurements on the sample step are removed with the first measurement on the step being left. Second, the measurements are interpolated into one second sample time. The processed measurements are the OCV, HPPC charge and discharge and ferry load profile measurements. The comparison between the data before and after processing is found in appendix A.

5.1 SOC-OCV function

The SOC-OCV function is fitted onto the processed data of the OCV measurement. A linear SOC-OCV function is required for the SSKF, a non-linear function can be used for the EKF. In order to fit a polynomial to the data, the OCV curve as a function of the SOC has to be identified. The measured terminal voltages have voltage losses caused by the battery's impedance. The voltage losses are corrected by using the resistance of the battery. The measured resistance was 40.3657 mΩ. The resistance was measured by using the EIS at 50 % SOC at a frequency of 398.089 Hz. There the reactance of the battery was close to zero, the exact measured reactance being 119.3854 μΩ. The corrected charging, discharging and average voltages are in Figure 21.

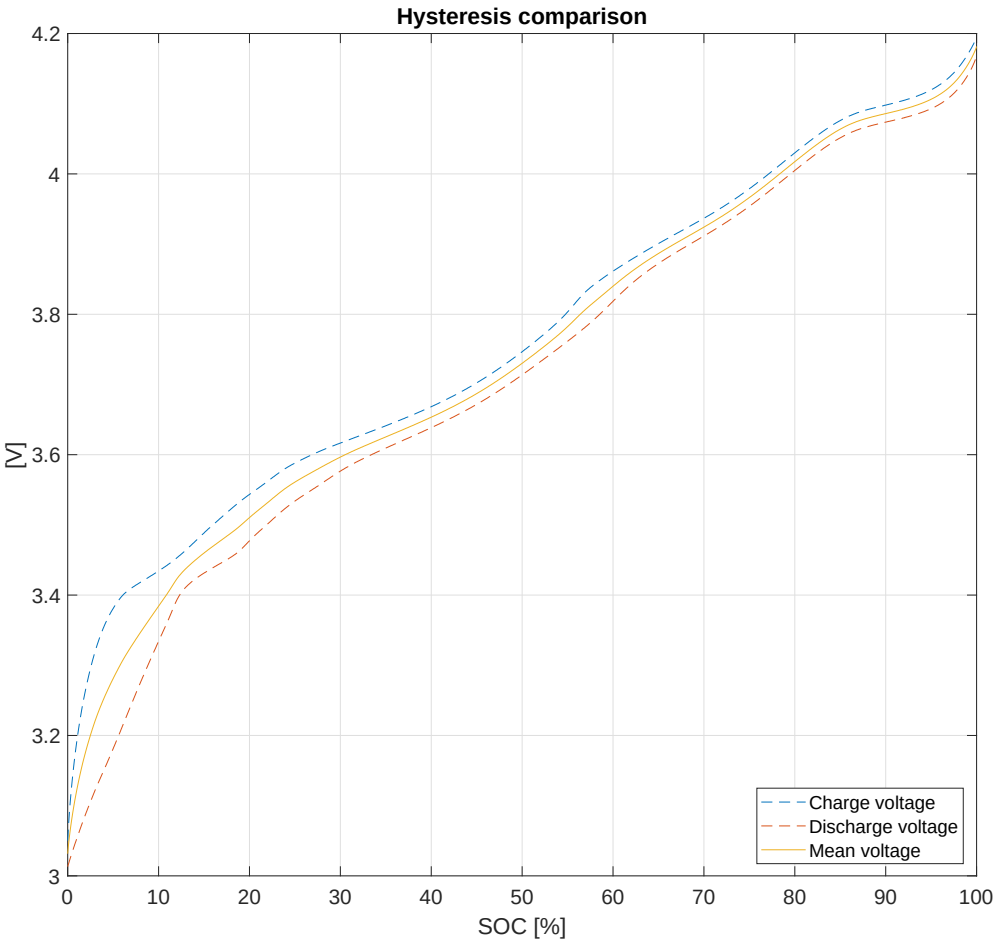

Figure 21: Voltages while charging and discharging at different SOC levels.

From the figure we can see that the hysteresis decreases as the SOC increases. The average hysteresis is 0.0493 V with the Ohmic losses averaging at 0.0121 V. It needs to be noted that the internal resistance of the battery is a function of the SOC, causing inaccuracy when the SOC differs from the 50 %.

The SOC-OCV function is fitted to the averaged voltage data to take into account the hysteresis present in the LiB. In order to determine which polynomial order provides the best fit for the non-linear SOC-OCV function, polynomial functions of degrees 1–12 are fitted into the data using least-squares methodology. The polynomial coefficients are found in appendix B. Root-mean-square error (RMSE) and mean absolute percentage error (MAPE) are compared in Figure 22 and the values can be found in appendix C.

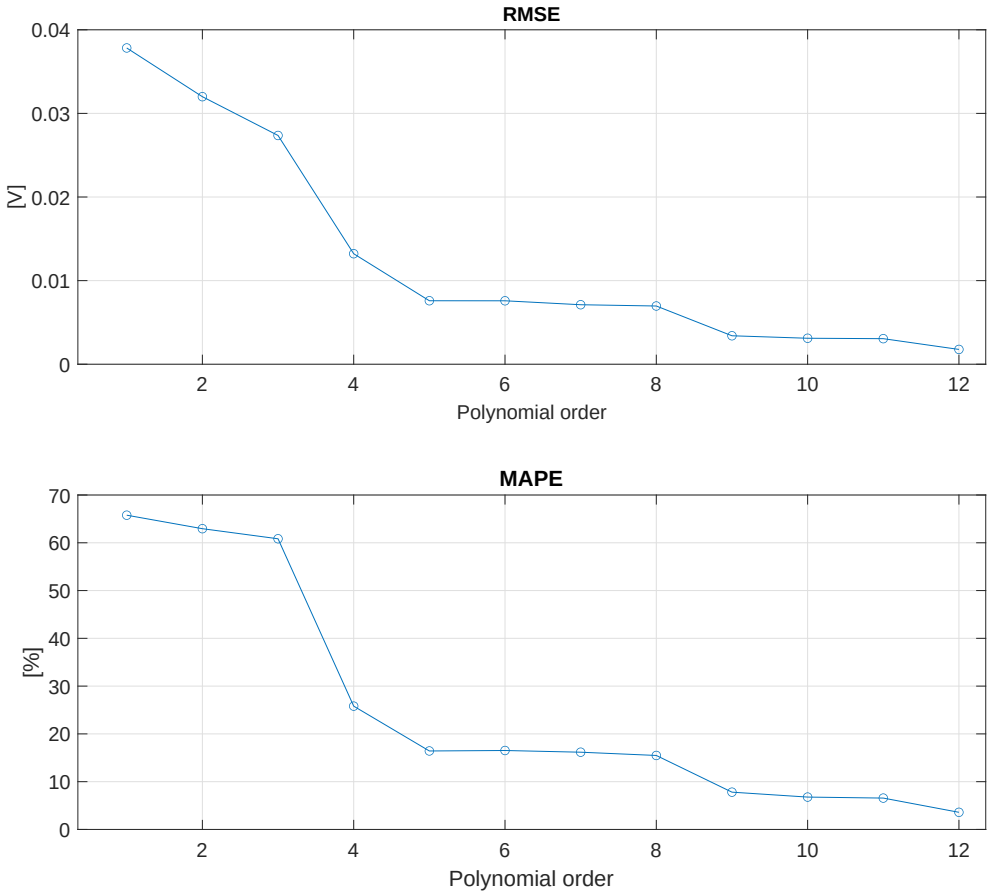

Figure 22: RMSE and MAPE of SOC-OCV fits for polynomial orders between 1–12.

The RMSE and MAPE decrease as the polynomial order increases. The RMSE and MAPE curves have almost exactly the same shape expect for the first three polynomial orders, with the MAPE being less steep than the RMSE. While the overall accuracy increases, the outliers do not decrease at the same pace for the first three polynomials because the MAPE is less steep than the RMSE. The ninth order polynomial is selected for the EKF because after it, a increase in polynomial order does not decrease the errors significantly. And with the computing power of a PLC, the computing overhead should be as low as possible. Visual comparison of the measurement average and the first and ninth order polynomial functions are in Figure 23.

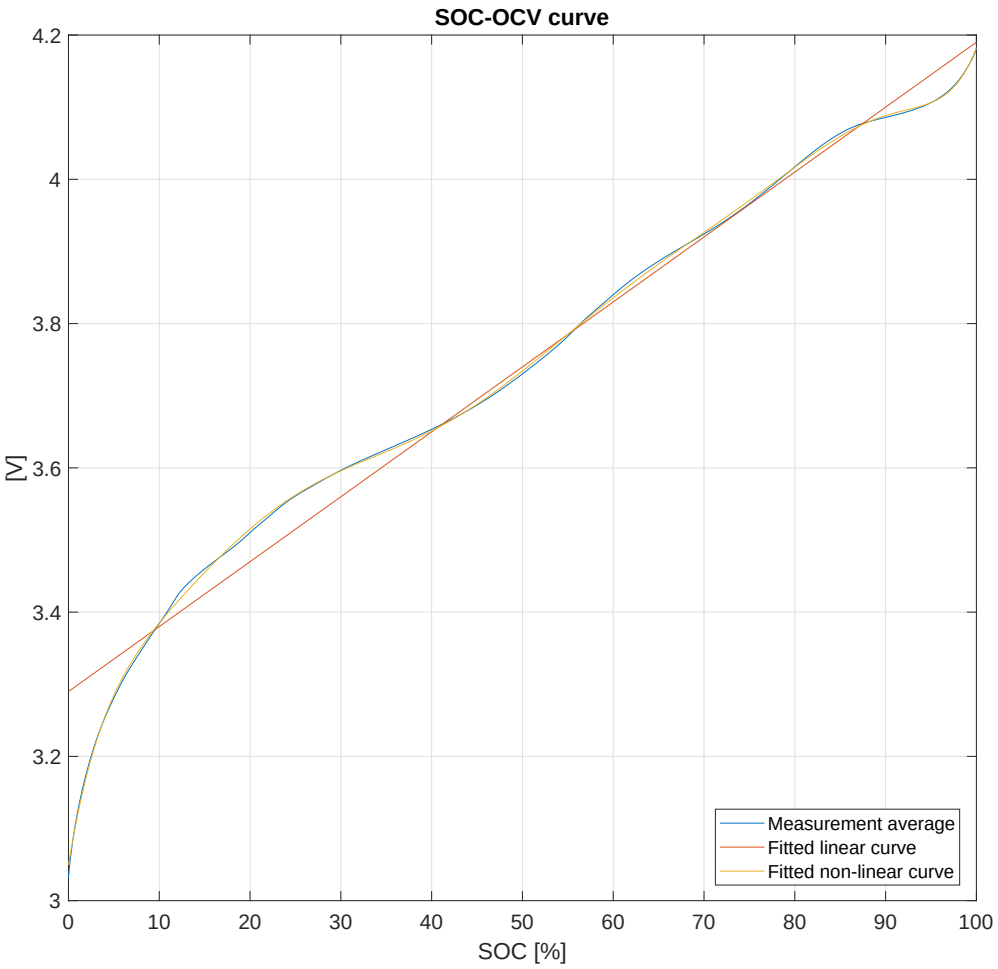

Figure 23: Comparison of measurement average and fitted linear function and non-linear function.

Visually the 9th order polynomial is quite close to the measurement, while the linear polynomial is clearly not. The linear function is the closest to the measured curve in the 40 % – 85 % SOC range. The discrepancy between the linear function and the measured curve increases the uncertainty in the SSKF SOC estimate.

5.2 ARX parameterization

Before parameterizing the ARX model, the data needs to be detrended. The detrending is done to remove linear trends and offsets e.g. the OCV so that only the dynamics are captured into the ARX model. The sample pulses are the pulses done at 100 % SOC. The pulses and detrend comparison is in the Figure 24.

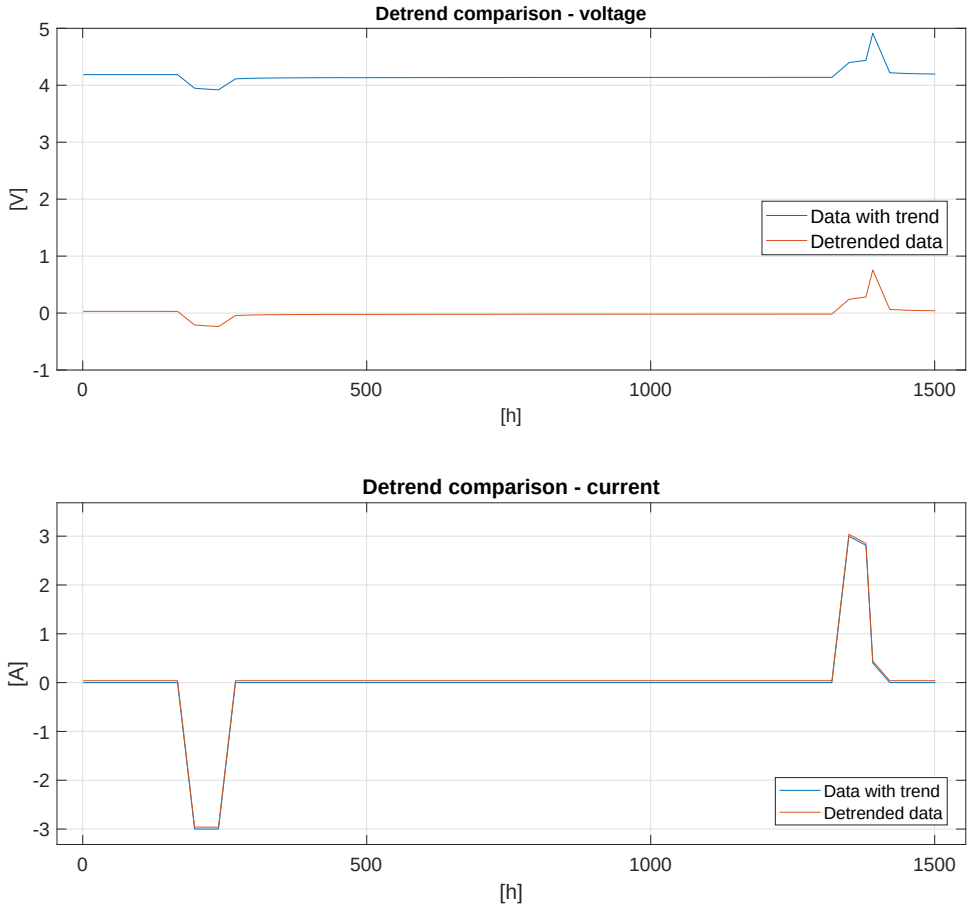

Figure 24: Trended and detrended current and voltage pulses.

Detrending the data removes the offset from the voltage measurement, leaving only the pulses. Current is not affected. From the detrended data, a second-order ARX model is parameterized by using the `arx` function in MATLAB. ARX model coefficients are presented in Table 1.

Table 1: ARX model parameters.

a_1	-1.89091496455494
a_2	0.898094120905121
b_0	-0.0103062170209651
b_1	0.0110950576985166

These parameters are then substituted into Equation 3.5 along with the SOC-OCV function coefficients, sampletime $T_s = 1$ s and $Q_{max} = 3.1352$ Ah. The Coulombic efficiency η is presumed to be 1. The HPPC discharge test current profile is then fed to the linear and the non-linear model, with the linear model having the first-order and non-linear having ninth-order function of SOC-OCV. The results are in Figure 25.

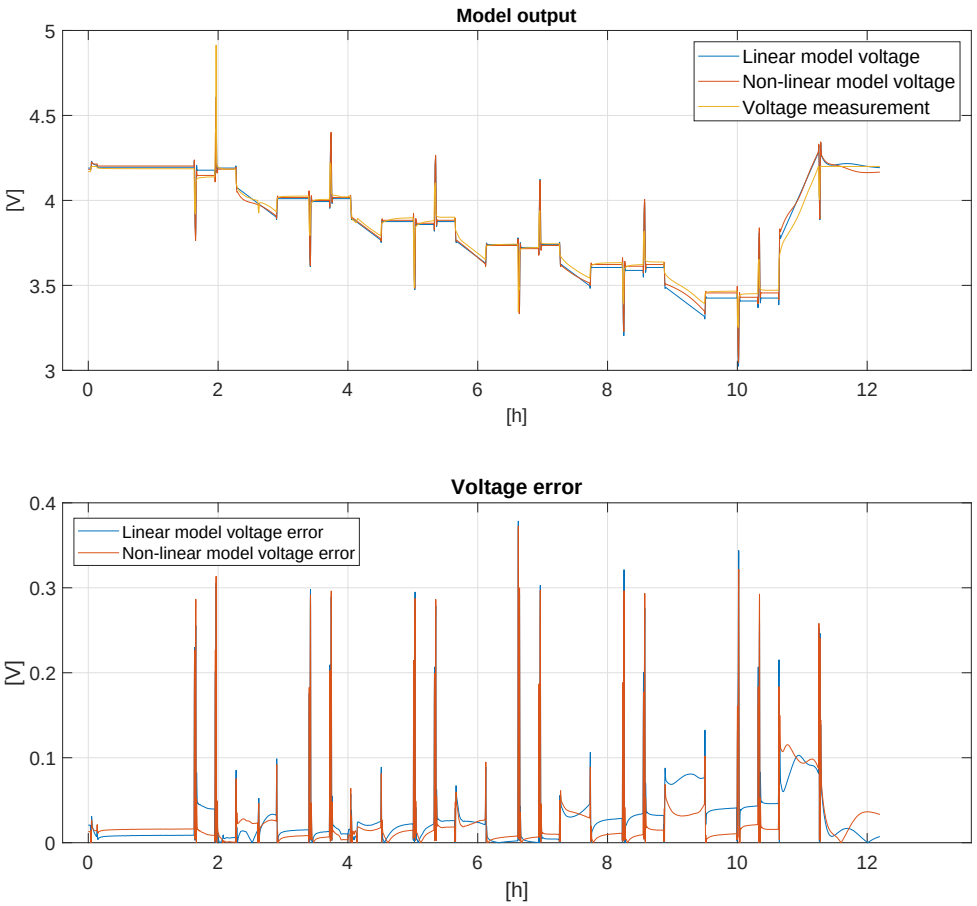

Figure 25: Model voltage output and absolute error.

From the figure it is not unambiguously clear that which one more accurate since at times one or other is more accurate. The linear model is clearly less accurate on pulses done at 100 %, 35 % and 15 % SOC. This is due to the linear SOC-OCV function differentiating from the measured SOC-OCV curve at those SOC levels. RMSE and MAPE for both the linear and the non-linear model outputs are in Table 2.

Table 2: RMSE and MAPE of the linear and the non-linear model.

	Linear model	Non-linear model
RMSE	0.414251223350806 V	0.394213738348390 V
MAPE	8.93386145670007 %	8.50982963906825 %

The difference between the linear and the non-linear model in RMSE and MAPE is slight but when using these metrics the non-linear model is more accurate.

5.3 Kalman filter validation

Before the SSKF can be used, the Kalman gain for it needs to be computed. By using MATLAB's `dlqr` function, the Kalman gain matrix L is computed. The computed SSKF Kalman gain using process noise covariance of 10 and measurement noise covariance of 0.1 is in Table 3.

Table 3: Kalman gain for the SSKF.

L_1	1.14452910853464
L_2	0.489065397418263
L_3	0.564076374611619

The Kalman gain is then substituted into Equation 3.6. The EKF requires initial guess for P_{cov} from where it starts converging on its final value. Initial guess $P_{cov} = 0.01$.

The first test is HPPC discharge test, Figure 26.

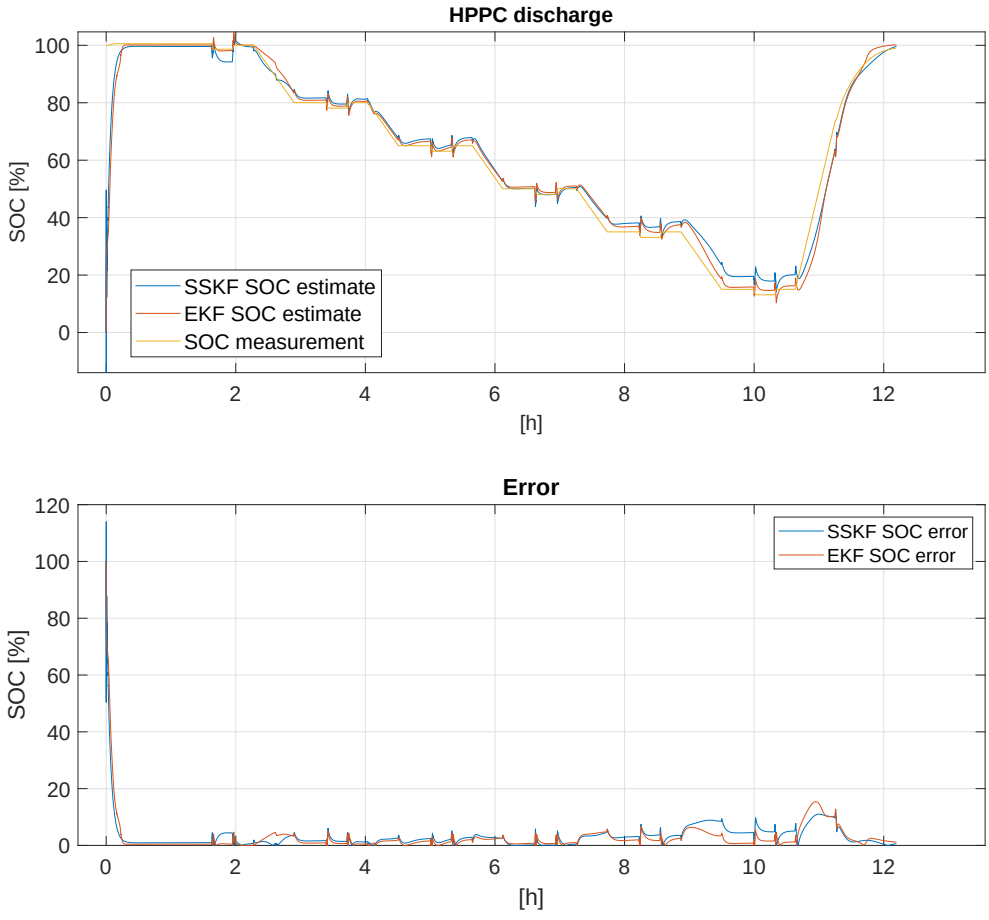

Figure 26: SOC estimate and absolute error.

The SOC estimate converges to the actual value from the initial guess of zero. It is hard to say that which is more accurate based on the graph. However, on the lover SOC, the SSKF deviates more from the measurement because of the less accurate linear SOC-OCV function. Both have absolute error of less than 20 pp after the estimate has converged from initial guess.

RMSE and MAPE for the test are in Table 4.

Table 4: RMSE and MAPE of the SSKF and the EKF from the HPPC discharge test.

	SSKF	EKF
RMSE	5.95485723206223 pp	6.18064697275087 pp
MAPE	8.88390439337589 %	5.90787100289788 %

Based on the RMSE and MAPE, the SSKF is generally more accurate but the outliers have higher deviation than with the EKF.

The next test is HPPC charging, Figure 27. It is done on a different battery cell so less accurate results are expected.

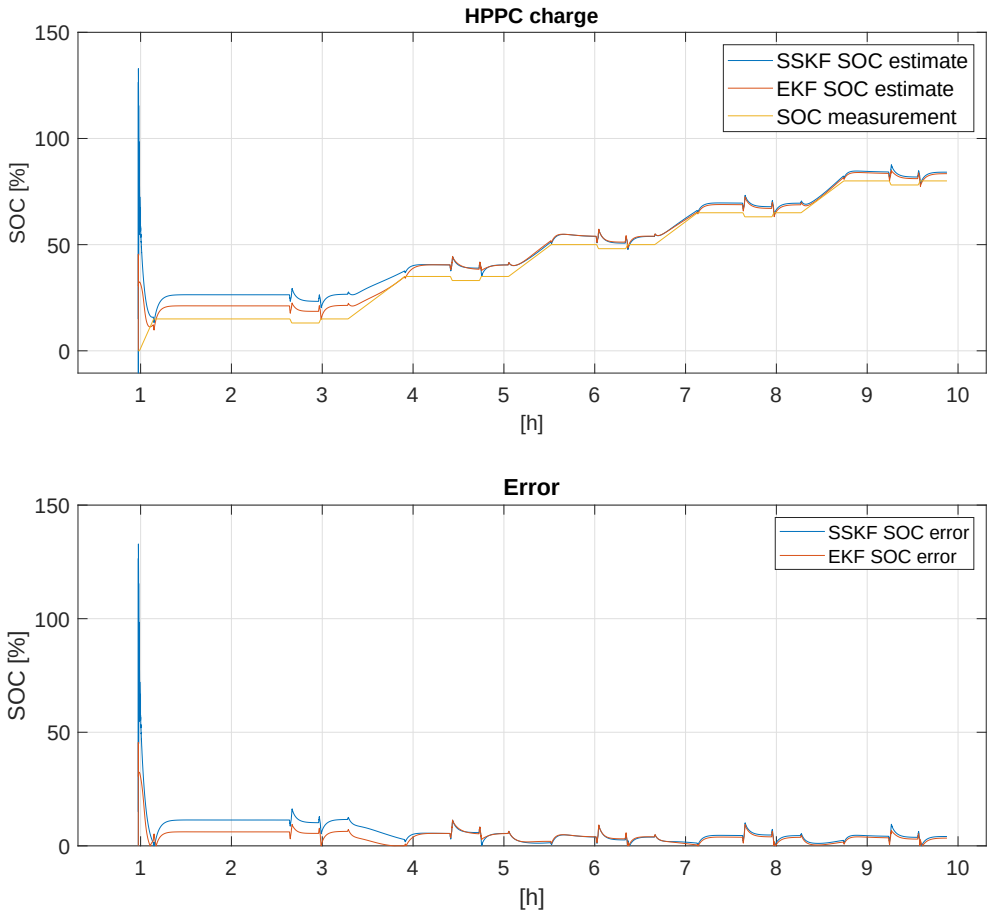

Figure 27: SOC estimate and absolute error.

On the lower SOC values, the error on the SSKF is higher when compared to the EKF. On the higher SOC levels, the estimates on both the SSKF and the EKF are almost hand in hand. Both have absolute error of less than 20 pp after the estimate has converged from the initial guess.

Table 5 contains RMSE of the test. MAPE could not be computed since the data included so many zero or near zero values.

Table 5: RMSE of the SSKF and the EKF from the HPPC charge test.

	SSKF	EKF
RMSE	8.26864351636635 pp	5.01310458447296 pp

Based on RMSE values, the EKF is more accurate.

The last test is the ferry load profile test, Figure 28. The test is done on same battery as the HPPC charge test.

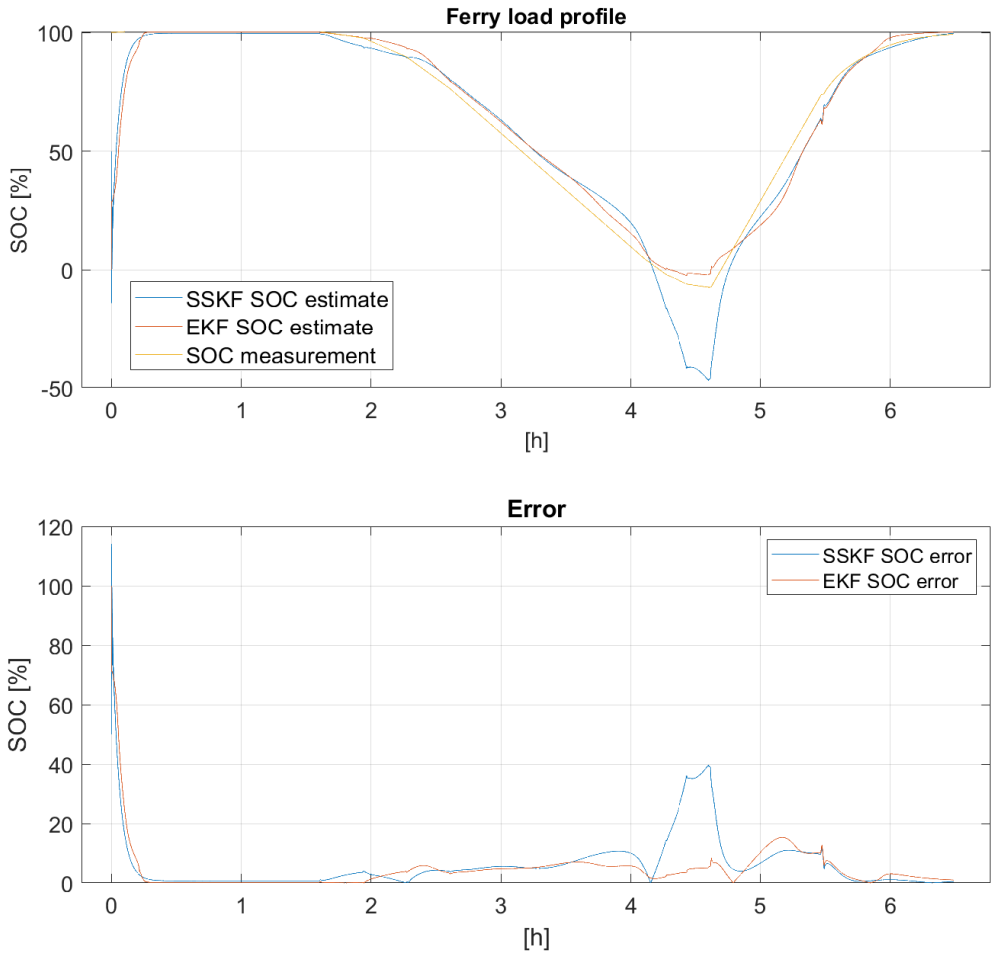

Figure 28: SOC estimate and absolute error.

The EKF is at almost every step either as accurate or more accurate than the SSKF after the SOC estimate has converged from the initial guess to when the SOC estimate goes under 20 %. The SOC estimate of the SSKF is almost -50 % when the SOC is under 20 %. This is due to the linear SOC-OCV function deviating from the actual curve at low SOC.

Table 6 has RMSE and MAPE.

Table 6: RMSE and MAPE of the SSKF and the EKF from the ferry load test.

	SSKF	EKF
RMSE	11.1613204933165 pp	8.55893815530564 pp
MAPE	125.020657558196 %	38.2247760964762 %

Metrics confirm what is visible on the graph. The EKF has generally a higher accuracy and less deviation in the outliers.

6 CONCLUSIONS

The objective of this thesis was to develop a SOC estimation method with a error rate of less than 20 % for the Danfoss marine team. A literature review of SOC estimation methods was conducted to select the best fitting estimation method for PLC use. The SSKF was selected as estimation method since it requires no matrix operations because the used PLC runtime does not have native support for them. The SSKF only supports linear systems and LiBs are non-linear. The EKF is also taken into examination to compare how the linearization for the SSKF affects the estimation results, and as a future-proofing if marine team ever decides to switch to industrial PCs from PLCs.

The KF based estimation requires a model of LiB to function. Battery's voltage depends on its charge, current and temperature, thus a function of SOC-OCV and a model of battery dynamics were implemented. A first-order and ninth-order polynomial functions were fitted into the SOC-OCV measurement, with the first-order being used for the SSKF and the ninth-order for the EKF. A second-order ARX model was selected since it provides the best balance between accuracy and computational overhead. A benefit of the ARX model is that it is already a discrete model, thus requiring no discretization because a programmatic implementation requires a discrete model. Another benefit of it is that it can be implemented as a online model as is.

The objective was successful with the both KFs performing well within error rate of 20 pp. The only exception being the ferry load profile test, where the SSKF had absolute error of 40 pp at its worst, while the EKF always stayed inside the set performance requirements.

The surprisingly good estimation accuracy of the SSKF adds interest to the future development of the linear KFs for SOC estimation in low computational power applications. Simple improvements to the SSKF include programmatically adding limits to the SOC value and offsets to the SOC-OCV functions when in certain SOC range to minimize linearization error.

An improvement to the model would be to parameterize the model and the SOC-OCV function at different temperatures. Now the model was only verified to work in constant room temperatures with no parameters for different temperatures, making the model accurate in room temperature.

Another thread for further research is to test the estimator on a real ferry. Ferries have battery packs, thus they also would be suitable environments to test the big cell model.

The biggest improvement would be to have more computational power on board a ship with either using cloud computing or having more local computational power. Cloud based solutions require internet, thus they are not usable when there is no reliable internet connection on a ship. The use of industrial PCs, which allows for matrix operations natively, would be the next choice. Having the ability to do matrix operations allows for the implementation of a non-linear KFs and computation of the Kalman gain online, which allows for the implementation of an online model. The online model allows the model to adapt to a aging battery.

REFERENCES

[1] W. Shen and R. Xiong, *Advanced Battery Management Technologies for Electric Vehicles*. Newark, UNITED KINGDOM: John Wiley & Sons, Incorporated, 2019, ISBN: 978-1-119-48167-6. [Online]. Available: http://ebookcentral.proquest.com/lib/lut/detail.action?docID=5630273 (visited on 05/04/2023).

[2] B. Kirby W., *Linden's Handbook of Batteries*. 2019, ISBN: 978-1-260-11593-2.

[3] X. Chen, W. Shen, T. T. Vo, Z. Cao, and A. Kapoor, "An overview of lithium-ion batteries for electric vehicles," in *2012 10th International Power & Energy Conference (IPEC)*, ISSN: 1947-1270, Dec. 2012, pp. 230–235. DOI: 10.1109/ASSCC.2012.6523269.

[4] X. Han, L. Lu, Y. Zheng, *et al.*, "A review on the key issues of the lithium ion battery degradation among the whole life cycle," *eTransportation*, vol. 1, p. 100 005, Aug. 2019, ISSN: 25901168. DOI: 10.1016/j.etran.2019.100005. [Online]. Available: https://linkinghub.elsevier.com/retrieve/pii/S2590116819300050 (visited on 07/10/2023).

[5] S. Zhang, X. Guo, X. Dou, and X. Zhang, "A data-driven coulomb counting method for state of charge calibration and estimation of lithium-ion battery," *Sustainable Energy Technologies and Assessments*, vol. 40, p. 100 752, Aug. 1, 2020, ISSN: 2213-1388. DOI: 10.1016/j.seta.2020.100752. [Online]. Available: https://www.sciencedirect.com/science/article/pii/S2213138820300527 (visited on 05/08/2023).

[6] Z. Cai, T. Pan, H. Jiang, Z. Li, and Y. Wang, "State-of-charge estimation of lithium-ion batteries based on ultrasonic detection," *Journal of Energy Storage*, vol. 65, p. 107 264, Aug. 15, 2023, ISSN: 2352-152X. DOI: 10.1016/j.est.2023.107264. [Online]. Available: https://www.sciencedirect.com/science/article/pii/S2352152X23006618 (visited on 05/09/2023).

[7] R. Xiong, J. Cao, Q. Yu, H. He, and F. Sun, "Critical review on the battery state of charge estimation methods for electric vehicles," *IEEE Access*, vol. 6, pp. 1832–1843, 2018, Conference Name: IEEE Access, ISSN: 2169-3536. DOI: 10.1109/ACCESS.2017.2780258.

[8] G. S. Misyris, D. I. Doukas, T. A. Papadopoulos, D. P. Labridis, and V. G. Agelidis, "State-of-charge estimation for li-ion batteries: A more accurate hybrid approach," *IEEE Transactions on Energy Conversion*, vol. 34, no. 1, pp. 109–119, Mar. 2019, Conference Name: IEEE Transactions on Energy Conversion, ISSN: 1558-0059. DOI: 10.1109/TEC.2018.2861994.

[9] S. Yang, X. Liu, S. Li, and C. Zhang, *Advanced Battery Management System for Electric Vehicles* (Key Technologies on New Energy Vehicles). Singapore: Springer Nature, 2023, ISBN: 978-981-19348-9-6 978-981-19349-0-2. DOI: 10.1007/978-981-19-3490-2. [Online]. Available: https://link.springer.com/10.1007/978-981-19-3490-2 (visited on 05/04/2023).

[10] R. Zhang, B. Xia, B. Li, *et al.*, "State of the art of lithium-ion battery SOC estimation for electrical vehicles," *Energies*, vol. 11, no. 7, p. 1820, Jul. 2018, Number: 7 Publisher: Multidisciplinary Digital Publishing Institute, ISSN: 1996-1073. DOI: 10.3390/en11071820. [Online]. Available: https://www.mdpi.com/1996-1073/11/7/1820 (visited on 12/07/2023).

[11] P. Weicker, *A Systems Approach to Lithium-Ion Battery Management*. Norwood, UNITED STATES: Artech House, 2013, ISBN: 978-1-60807-660-4. [Online]. Available: http://ebookcentral.proquest.com/lib/lut/detail.action?docID=1463546 (visited on 05/04/2023).

[12] J. Lee and J. Won, "Enhanced coulomb counting method for SoC and SoH estimation based on coulombic efficiency," *IEEE Access*, vol. 11, pp. 15 449–15 459, 2023, Conference Name: IEEE Access, ISSN: 2169-3536. DOI: 10.1109/ACCESS.2023.3244801.

[13] K. S. Ng, C.-S. Moo, Y.-P. Chen, and Y.-C. Hsieh, "Enhanced coulomb counting method for estimating state-of-charge and state-of-health of lithium-ion batteries," *Applied Energy*, vol. 86, no. 9, pp. 1506–1511, Sep. 1, 2009, ISSN: 0306-2619. DOI: 10.1016/j.apenergy.2008.11.021. [Online]. Available: https://www.sciencedirect.com/science/article/pii/S0306261908003061 (visited on 05/09/2023).

[14] F. Mohammadi, "Lithium-ion battery state-of-charge estimation based on an improved coulomb-counting algorithm and uncertainty evaluation," *Journal of Energy Storage*, vol. 48, p. 104 061, Apr. 1, 2022, ISSN: 2352-152X. DOI: 10.1016/j.est.2022.104061. [Online]. Available: https://www.sciencedirect.com/science/article/pii/S2352152X22000986 (visited on 05/08/2023).

[15] B. Pattipati, B. Balasingam, G. V. Avvari, K. R. Pattipati, and Y. Bar-Shalom, "Open circuit voltage characterization of lithium-ion batteries," *Journal of Power Sources*, vol. 269, pp. 317–333, Dec. 10, 2014, ISSN: 0378-7753. DOI: 10.1016/j.jpowsour.2014.06.152. [Online]. Available: https://www.sciencedirect.com/science/article/pii/S037877531401026X (visited on 05/04/2023).

[16] A. Hentunen, T. Lehmuspelto, and J. Suomela, "Time-domain parameter extraction method for thévenin-equivalent circuit battery models," *IEEE Transactions on Energy Conversion*, vol. 29, no. 3, pp. 558–566, Sep. 2014, Conference Name: IEEE Transactions on Energy Conversion, ISSN: 1558-0059. DOI: 10.1109/TEC.2014.2318205.

[17] J. Turner, "3. simplified extended kalman filter observer for SOC estimation of commercial power-oriented LFP lithium battery cells (2013-01-1544)," in *Progress in Modeling and Simulation of Batteries*, Conference Name: Progress in Modeling and Simulation of Batteries, SAE, 2016, pp. 19–28, ISBN: 978-0-7680-8366-8. [Online]. Available: https://ieeexplore.ieee.org/document/8504691 (visited on 05/04/2023).

[18] Z. Wang, G. Feng, D. Zhen, F. Gu, and A. Ball, "A review on online state of charge and state of health estimation for lithium-ion batteries in electric vehicles," *Energy Reports*, vol. 7, pp. 5141–5161, Nov. 1, 2021, ISSN: 2352-4847. DOI: 10.1016/j.egyr.2021.08.113. [Online]. Available: https://www.sciencedirect.com/science/article/pii/S2352484721007150 (visited on 05/10/2023).

[19] P. Eleftheriadis, A. Dolara, and S. Leva, "An overview of data-driven methods for the online state of charge estimation," in *2022 IEEE International Conference on Environment and Electrical Engineering and 2022 IEEE Industrial and Commercial Power Systems Europe (EEEIC / I&CPS Europe)*, Jun. 2022, pp. 1–6. DOI: 10.1109/EEEIC/ICPSEurope54979.2022.9854413.

[20] D. N. T. How, M. A. Hannan, M. S. Hossain Lipu, and P. J. Ker, "State of charge estimation for lithium-ion batteries using model-based and data-driven methods: A review," *IEEE Access*, vol. 7, pp. 136 116–136 136, 2019, Conference Name: IEEE Access, ISSN: 2169-3536. DOI: 10.1109/ACCESS.2019.2942213.

[21] M. Hossain Lipu, M. Hannan, A. Hussain, *et al.*, "Data-driven state of charge estimation of lithium-ion batteries: Algorithms, implementation factors, limitations and future trends," *Journal of Cleaner Production*, vol. 277, p. 124 110, Dec. 2020, ISSN: 09596526. DOI: 10.1016/j.jclepro.2020.124110. [Online]. Available: https://linkinghub.elsevier.com/retrieve/pii/S095965262034155X (visited on 05/05/2023).

[22] *Linden's Handbook of Batteries, Fourth Edition*, Fourth Edition. McGraw-Hill Education, 2011, ISBN: 978-0-07-162421-3. [Online]. Available: https://www.accessengineeringli
com/content/book/9780071624213 (visited on 05/12/2023).

[23] K. A. Smith, C. D. Rahn, and C.-Y. Wang, "Control oriented 1d electrochemical model of lithium ion battery," *Energy Conversion and Management*, vol. 48, no. 9, pp. 2565–2578, Sep. 1, 2007, ISSN: 0196-8904. DOI: 10.1016/j.enconman.2007.03.015. [Online]. Available: https://www.sciencedirect.com/science/article/pii/S0196890407000908 (visited on 05/12/2023).

[24] N. Lotfi, R. G. Landers, J. Li, and J. Park, "Reduced-order electrochemical model-based SOC observer with output model uncertainty estimation," *IEEE Transactions on Control Systems Technology*, vol. 25, no. 4, pp. 1217–1230, Jul. 2017, Conference

Name: IEEE Transactions on Control Systems Technology, ISSN: 1558-0865. DOI: 10.1109/TCST.2016.2598764.

[25] X. Hu, S. Li, and H. Peng, "A comparative study of equivalent circuit models for li-ion batteries," *Journal of Power Sources*, vol. 198, pp. 359–367, Jan. 15, 2012, ISSN: 0378-7753. DOI: 10.1016/j.jpowsour.2011.10.013. [Online]. Available: https://www.sciencedirect.com/science/article/pii/S0378775311019628 (visited on 05/04/2023).

[26] X. Lai, Y. Zheng, and T. Sun, "A comparative study of different equivalent circuit models for estimating state-of-charge of lithium-ion batteries," *Electrochimica Acta*, vol. 259, pp. 566–577, Jan. 1, 2018, ISSN: 0013-4686. DOI: 10.1016/j.electacta.2017.10.153. [Online]. Available: https://www.sciencedirect.com/science/article/pii/S0013468617322880 (visited on 05/19/2023).

[27] X. Zhao, Y. Cai, L. Yang, Z. Deng, and J. Qiang, "State of charge estimation based on a new dual-polarization-resistance model for electric vehicles," *Energy*, vol. 135, pp. 40–52, Sep. 15, 2017, ISSN: 0360-5442. DOI: 10.1016/j.energy.2017.06.094. [Online]. Available: https://www.sciencedirect.com/science/article/pii/S0360544217310885 (visited on 05/22/2023).

[28] T. Hu, B. Zanchi, and J. Zhao, "Simple analytical method for determining parameters of discharging batteries," *IEEE Transactions on Energy Conversion*, vol. 26, no. 3, pp. 787–798, Sep. 2011, Conference Name: IEEE Transactions on Energy Conversion, ISSN: 1558-0059. DOI: 10.1109/TEC.2011.2129594.

[29] X. Lai, W. Gao, Y. Zheng, *et al.*, "A comparative study of global optimization methods for parameter identification of different equivalent circuit models for li-ion batteries," *Electrochimica Acta*, vol. 295, pp. 1057–1066, Feb. 1, 2019, ISSN: 0013-4686. DOI: 10.1016/j.electacta.2018.11.134. [Online]. Available: https://www.sciencedirect.com/science/article/pii/S0013468618326173 (visited on 05/19/2023).

[30] N. Biju and H. Fang, "BattX: An equivalent circuit model for lithium-ion batteries over broad current ranges," *Applied Energy*, vol. 339, p. 120 905, Jun. 1, 2023, ISSN: 0306-2619. DOI: 10.1016/j.apenergy.2023.120905. [Online]. Available: https://www.sciencedirect.com/science/article/pii/S0306261923002696 (visited on 05/11/2023).

[31] S. Yuan, H. Wu, and C. Yin, "State of charge estimation using the extended kalman filter for battery management systems based on the ARX battery model," *Energies*, vol. 6, no. 1, pp. 444–470, Jan. 2013, Number: 1 Publisher: Multidisciplinary Digital Publishing Institute, ISSN: 1996-1073. DOI: 10.3390/en6010444. [Online]. Available: https://www.mdpi.com/1996-1073/6/1/444 (visited on 08/02/2023).

[32] X.-K. Chen and D. Sun, "Modeling and state of charge estimation of lithium-ion battery," *Advances in Manufacturing*, vol. 3, no. 3, pp. 202–211, Sep. 1, 2015, ISSN: 2195-3597. DOI: 10.1007/s40436-015-0116-3. [Online]. Available: https://doi.org/10.1007/s40436-015-0116-3 (visited on 05/09/2023).

[33] V. H. Johnson, "Battery performance models in ADVISOR," *Journal of Power Sources*, vol. 110, no. 2, pp. 321–329, Aug. 22, 2002, ISSN: 0378-7753. DOI: 10.1016/S0378-7753(02)00194-5. [Online]. Available: https://www.sciencedirect.com/science/article/pii/S0378775302001945 (visited on 10/31/2023).

[34] G. L. Plett, "Extended kalman filtering for battery management systems of LiPB-based HEV battery packs: Part 2. modeling and identification," *Journal of Power Sources*, vol. 134, no. 2, pp. 262–276, Aug. 12, 2004, ISSN: 0378-7753. DOI: 10.1016/j.jpowsour.2004.02.032. [Online]. Available: https://www.sciencedirect.com/science/article/pii/S037877530400360X (visited on 05/17/2023).

[35] J. Xu, C. C. Mi, B. Cao, and J. Cao, "A new method to estimate the state of charge of lithium-ion batteries based on the battery impedance model," *Journal of Power Sources*, vol. 233, pp. 277–284, Jul. 1, 2013, ISSN: 0378-7753. DOI: 10.1016/j.jpowsour.2013.01.094. [Online]. Available: https://www.sciencedirect.com/science/article/pii/S0378775313001432 (visited on 05/09/2023).

[36] X. Wang, X. Wei, J. Zhu, *et al.*, "A review of modeling, acquisition, and application of lithium-ion battery impedance for onboard battery management," *eTransportation*, vol. 7, p. 100 093, Feb. 2021, ISSN: 25901168. DOI: 10.1016/j.etran.2020.100093. [Online]. Available: https://linkinghub.elsevier.com/retrieve/pii/S2590116820300515 (visited on 05/26/2023).

[37] D. Andre, M. Meiler, K. Steiner, C. Wimmer, T. Soczka-Guth, and D. U. Sauer, "Characterization of high-power lithium-ion batteries by electrochemical impedance spectroscopy. i. experimental investigation," *Journal of Power Sources*, Selected papers presented at the 12th Ulm ElectroChemical Talks (UECT):2015 Technologies on Batteries and Fuel Cells, vol. 196, no. 12, pp. 5334–5341, Jun. 15, 2011, ISSN: 0378-7753. DOI: 10.1016/j.jpowsour.2010.12.102. [Online]. Available: https://www.sciencedirect.com/science/article/pii/S0378775311000681 (visited on 05/24/2023).

[38] D. Andre, M. Meiler, K. Steiner, H. Walz, T. Soczka-Guth, and D. U. Sauer, "Characterization of high-power lithium-ion batteries by electrochemical impedance spectroscopy. II: Modelling," *Journal of Power Sources*, Selected papers presented at the 12th Ulm ElectroChemical Talks (UECT):2015 Technologies on Batteries and Fuel Cells, vol. 196, no. 12, pp. 5349–5356, Jun. 15, 2011, ISSN: 0378-7753. DOI: 10.1016/j.jpowsour.2010.07.071. [Online]. Available: https://www.sciencedirect.com/science/article/pii/S0378775310012942 (visited on 05/09/2023).

[39] S. Skoog and S. David, "Parameterization of linear equivalent circuit models over wide temperature and SOC spans for automotive lithium-ion cells using electrochemical impedance spectroscopy," *Journal of Energy Storage*, vol. 14, pp. 39–48, Dec. 1, 2017, ISSN: 2352-152X. DOI: 10.1016/j.est.2017.08.004. [Online]. Available: https://www.sciencedirect.com/science/article/pii/S2352152X16301906 (visited on 05/11/2023).

[40] J. Sihvo, D.-I. Stroe, T. Messo, and T. Roinila, "Fast approach for battery impedance identification using pseudo-random sequence signals," *IEEE Transactions on Power Electronics*, vol. 35, no. 3, pp. 2548–2557, Mar. 2020, Conference Name: IEEE Transactions on Power Electronics, ISSN: 1941-0107. DOI: 10.1109/TPEL.2019.2924286.

[41] J. Xu, C. C. Mi, B. Cao, J. Deng, Z. Chen, and S. Li, "The state of charge estimation of lithium-ion batteries based on a proportional-integral observer," *IEEE Transactions on Vehicular Technology*, vol. 63, no. 4, pp. 1614–1621, May 2014, Conference Name: IEEE Transactions on Vehicular Technology, ISSN: 1939-9359. DOI: 10.1109/TVT.2013.2287375.

[42] X. Hu, F. Sun, and Y. Zou, "Estimation of state of charge of a lithium-ion battery pack for electric vehicles using an adaptive luenberger observer," *Energies*, vol. 3, no. 9, pp. 1586–1603, Sep. 2010, Number: 9 Publisher: Molecular Diversity Preservation International, ISSN: 1996-1073. DOI: 10.3390/en3091586. [Online]. Available: https://www.mdpi.com/1996-1073/3/9/1586 (visited on 08/28/2023).

[43] J. Li, J. Klee Barillas, C. Guenther, and M. A. Danzer, "A comparative study of state of charge estimation algorithms for LiFePO4 batteries used in electric vehicles," *Journal of Power Sources*, vol. 230, pp. 244–250, May 2013, ISSN: 03787753. DOI: 10.1016/j.jpowsour.2012.12.057. [Online]. Available: https://linkinghub.elsevier.com/retrieve/pii/S0378775312019039 (visited on 08/16/2023).

[44] I.-S. Kim, "The novel state of charge estimation method for lithium battery using sliding mode observer," *Journal of Power Sources*, Special issue including selected papers presented at the Second International Conference on Polymer Batteries and Fuel Cells together with regular papers, vol. 163, no. 1, pp. 584–590, Dec. 7, 2006, ISSN: 0378-7753. DOI: 10.1016/j.jpowsour.2006.09.006. [Online]. Available: https://www.sciencedirect.com/science/article/pii/S0378775306018349 (visited on 10/19/2023).

[45] R. Xiong, Q. Yu, L. Y. Wang, and C. Lin, "A novel method to obtain the open circuit voltage for the state of charge of lithium ion batteries in electric vehicles by using h infinity filter," *Applied Energy*, Transformative Innovations for a Sustainable Future – Part II, vol. 207, pp. 346–353, Dec. 1, 2017, ISSN: 0306-2619. DOI: 10.1016/j.apenergy.2017.05.136. [Online]. Available: https://www.sciencedirect.com/science/article/pii/S0306261917306852 (visited on 10/18/2023).

[46] G. L. Plett, "Extended kalman filtering for battery management systems of LiPB-based HEV battery packs: Part 1. background," *Journal of Power Sources*, vol. 134, no. 2, pp. 252–261, Aug. 12, 2004, ISSN: 0378-7753. DOI: 10.1016/j.jpowsour.2004.02.031. [Online]. Available: https://www.sciencedirect.com/science/article/pii/S0378775304003593 (visited on 05/24/2023).

[47] P. Shrivastava, T. K. Soon, M. Y. I. B. Idris, and S. Mekhilef, "Overview of model-based online state-of-charge estimation using kalman filter family for lithium-ion batteries," *Renewable and Sustainable Energy Reviews*, vol. 113, p. 109 233, Oct. 1, 2019, ISSN: 1364-0321. DOI: 10.1016/j.rser.2019.06.040. [Online]. Available: https://www.sciencedirect.com/science/article/pii/S1364032119304332 (visited on 05/19/2023).

[48] G. L. Plett, "Extended kalman filtering for battery management systems of LiPB-based HEV battery packs: Part 3. state and parameter estimation," *Journal of Power Sources*, vol. 134, no. 2, pp. 277–292, Aug. 12, 2004, ISSN: 0378-7753. DOI: 10.1016/j.jpowsour.2004.02.033. [Online]. Available: https://www.sciencedirect.com/science/article/pii/S0378775304003611 (visited on 08/16/2023).

[49] N. Assimakis and M. Adam, "Iterative and algebraic algorithms for the computation of the steady state kalman filter gain," *International Scholarly Research Notices*, vol. 2014, e417623, May 4, 2014, Publisher: Hindawi. DOI: 10.1155/2014/417623. [Online]. Available: https://www.hindawi.com/journals/isrn/2014/417623/ (visited on 11/15/2023).

[50] G. L. Plett, "Sigma-point kalman filtering for battery management systems of LiPB-based HEV battery packs: Part 1: Introduction and state estimation," *Journal of Power Sources*, vol. 161, no. 2, pp. 1356–1368, Oct. 27, 2006, ISSN: 0378-7753. DOI: 10.1016/j.jpowsour.2006.06.003. [Online]. Available: https://www.sciencedirect.com/science/article/pii/S0378775306011414 (visited on 05/24/2023).

[51] I. Arasaratnam and S. Haykin, "Cubature kalman filters," *IEEE Transactions on Automatic Control*, vol. 54, no. 6, pp. 1254–1269, Jun. 2009, Conference Name: IEEE Transactions on Automatic Control, ISSN: 1558-2523. DOI: 10.1109/TAC.2009.2019800.

[52] J. Linghu, L. Kang, M. Liu, X. Luo, Y. Feng, and C. Lu, "Estimation for state-of-charge of lithium-ion battery based on an adaptive high-degree cubature kalman filter," *Energy*, vol. 189, p. 116 204, Dec. 2019, ISSN: 03605442. DOI: 10.1016/j.energy.2019.116204. [Online]. Available: https://linkinghub.elsevier.com/retrieve/pii/S0360544219318997 (visited on 06/14/2023).

[53] F. Sun and R. Xiong, "A novel dual-scale cell state-of-charge estimation approach for series-connected battery pack used in electric vehicles," *Journal of Power Sources*, vol. 274, pp. 582–594, Jan. 2015, ISSN: 03787753. DOI: 10.1016/j.jpowsour.2014.

10.119. [Online]. Available: https://linkinghub.elsevier.com/retrieve/pii/S0378775314017285 (visited on 08/22/2023).

[54] S. Zhou, Z. Chen, D. Huang, and T. Lin, "A fault-tolerant SoC estimation method for series–parallel connected li-ion battery pack," *IEEE Transactions on Power Electronics*, vol. 36, no. 12, pp. 13 434–13 448, Dec. 2021, Conference Name: IEEE Transactions on Power Electronics, ISSN: 1941-0107. DOI: 10.1109/TPEL.2021.3086555.

[55] D. Zhang, L. D. Couto, S. Benjamin, W. Zeng, D. F. Coutinho, and S. J. Moura, "State of charge estimation of parallel connected battery cells via descriptor system theory," in *2020 American Control Conference (ACC)*, ISSN: 2378-5861, Jul. 2020, pp. 2207–2212. DOI: 10.23919/ACC45564.2020.9147284.

[56] Q. Yu, Y. Huang, A. Tang, C. Wang, and W. Shen, "OCV-SOC-temperature relationship construction and state of charge estimation for a series– parallel lithium-ion battery pack," *IEEE Transactions on Intelligent Transportation Systems*, vol. 24, no. 6, pp. 6362–6371, Jun. 2023, Conference Name: IEEE Transactions on Intelligent Transportation Systems, ISSN: 1558-0016. DOI: 10.1109/TITS.2023.3252164.

[57] X. Huang, X. Feng, X. Han, L. Lu, and M. Ouyang, "Study on modeling, experimentation and state of charge estimation of parallel connected lithium-ion batteries," *International Journal of Electrochemical Science*, vol. 15, no. 2, pp. 1264–1286, Feb. 2020, ISSN: 14523981. DOI: 10.20964/2020.02.02. [Online]. Available: https://linkinghub.elsevier.com/retrieve/pii/S1452398123103178 (visited on 08/24/2023).

[58] X. Liu, W. Li, and A. Zhou, "PNGV equivalent circuit model and SOC estimation algorithm for lithium battery pack adopted in AGV vehicle," *IEEE Access*, vol. 6, pp. 23 639–23 647, 2018, Conference Name: IEEE Access, ISSN: 2169-3536. DOI: 10.1109/ACCESS.2018.2812421.

[59] "Estimate parameters of ARX, ARIX, AR, or ARI model - MATLAB arx - MathWorks nordic." (), [Online]. Available: https://se.mathworks.com/help/ident/ref/arx.html (visited on 12/15/2023).

[60] "Linear-quadratic (LQ) state-feedback regulator for discrete-time state-space system - MATLAB dlqr - MathWorks nordic." (), [Online]. Available: https://se.mathworks.com/help/control/ref/dlqr.html (visited on 12/15/2023).

A APPENDIX: ORIGINAL AND PROCESSED DATA

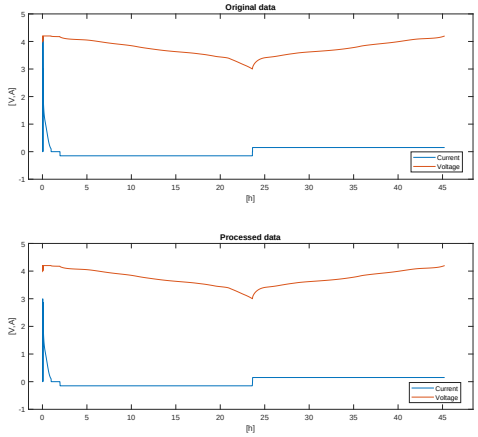

(a) OCV measurement original and processed.

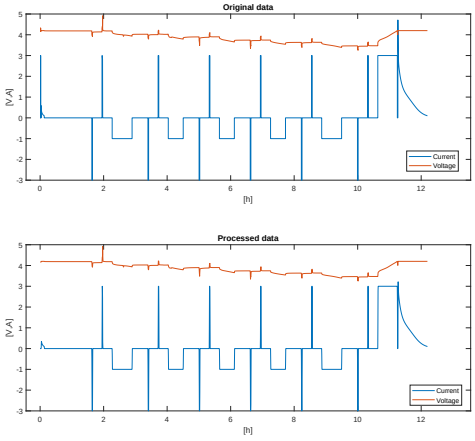

(b) HPPC discharge measurement original and processed.

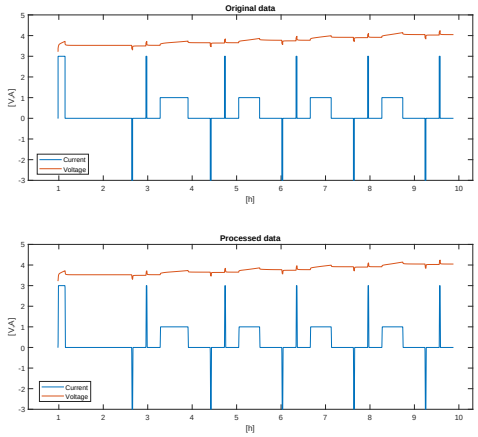

(a) HPPC charge measurement original and processed.

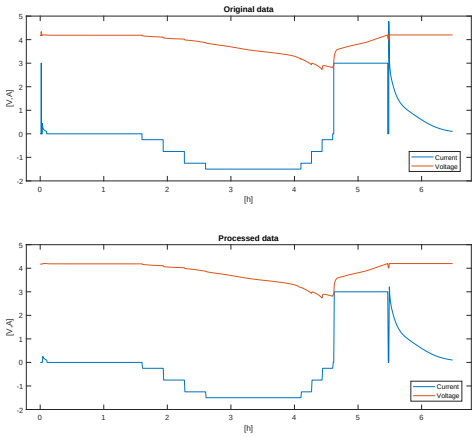

(b) Load profile measurement original and processed.

B APPENDIX: POLYNOMIALS

Table 7: Polynomial functions. Rows are the monomial order and the columns are polynomial order.

Order	1st	2nd	3rd
0	3.28991259974663	3.24481064470432	3.20090996375169
1	0.900148993773028	1.17076420429503	1.69758931387943
2	0	-0.270615210522001	-1.58768645355942
3	0	0	0.878047495358269

Order	4th	5th	6th
0	3.12905222875545	3.09317790914578	3.09213021408770
1	3.13482719008544	4.21115367281291	4.25516252497247
2	-8.05535393575844	-15.5898331049716	-16.0299386059104
3	10.9389067073443	31.0310449491154	32.7914952519099
4	-5.03042960599300	-27.6341577994363	-30.9350254639238
5	0	9.04149127737719	11.9462622930854
6	0	0	-0.968257005236064

Order	7th	8th	9th
0	3.08193912889169	3.07591089661387	3.04944137532010
1	4.82596239520239	5.26009282235009	7.64302392766467
2	-23.7361497740556	-31.3339696279505	-83.7631733988637
3	75.6047888872708	131.323925765178	620.683612234535
4	-148.672945612876	-357.623201927210	-2743.30535852121
5	181.489812080779	616.110257411403	7296.10619238788
6	-123.416638733349	-630.476153643833	-11763.8845183590
7	34.9852519223180	345.430423179698	11251.6689450688
8	0	-77.6112928143465	-5871.55982036722
9	0	0	1287.54411723532

Table 8: Polynomial functions continued.

Order	10th	11th	12th
0	3.05580292277019	3.05845616835803	3.04600759838695
1	6.94301064766904	6.59263579127139	8.53557467246898
2	-64.8607082412250	-53.4719877305219	-128.287159773527
3	402.243656491979	242.791317917818	1489.80705584807
4	-1405.32191966885	-209.386323791153	-11433.0186142059
5	2479.28323075604	-2878.62535361133	58179.5829068119
6	-1059.72207219898	14121.2280514499	-199586.229866624
7	-3603.17919518175	-31486.8002528406	465715.850350818
8	6662.26082685425	39774.2382240850	-737110.729965565
9	-4592.52829087432	-29119.9925397504	776542.291091710
10	1176.01448162306	11477.5627111488	-520260.973954469
11	0	-1873.00876895206	200275.762107253
12	0	0	-33691.4618127593

C APPENDIX: RMSE AND MAPE OF DIFFERENT POLYNOMIALS

Table 9: RMSE and MAPE of polynomial fits between orders of 1–12 for SOC-OCV.

Order	RMSE [V]	MAPE [%]
1	0.0378259959658505	0.657748348711405
2	0.0319990204115313	0.629496899719435
3	0.0273600175287123	0.608387612438446
4	0.0132172979223536	0.258100508701680
5	0.00759307805028733	0.164256168303787
6	0.00758751295842823	0.165230470115246
7	0.00711628298137629	0.161670692268763
8	0.00696432915733809	0.154850675243553
9	0.00340347162559559	0.0780414821949616
10	0.00310705361169594	0.0677380760543737
11	0.00305731707224788	0.0656446975342867
12	0.00177089340492720	0.0358730697194130